

TESE DE DOUTORADO Nº 360

**IMPULSE GROUND-PENETRATING RADAR ANTENNA DESIGN AND  
OPTIMIZATION FOR HOMOGENEOUS AND LOW-LOSS DIELECTRIC  
MULTILAYER MEDIA**

**Maria Victoria Africano Contreras**

DATA DA DEFESA: 14/04/2021

**Universidade Federal de Minas Gerais**

**Escola de Engenharia**

**Programa de Pós-Graduação em Engenharia Elétrica**

**IMPULSE GROUND-PENETRATING RADAR ANTENNA DESIGN  
AND OPTIMIZATION FOR HOMOGENEOUS AND LOW-LOSS  
DIELECTRIC MULTILAYER MEDIA**

Maria Victoria Africano Contreras

Tese de Doutorado submetida à Banca Examinadora designada pelo Colegiado do Programa de Pós-Graduação em Engenharia Elétrica da Escola de Engenharia da Universidade Federal de Minas Gerais, como requisito para obtenção do Título de Doutor em Engenharia Elétrica.

Orientador: Prof. Ricardo Luiz da Silva Adriano

Coorientador: Prof. Diogo Batista de Oliveira

Belo Horizonte - MG

Abril de 2021

A258i

Africano Contreras, Maria Victoria.

Impulse ground-penetrating radar antenna design and optimization for homogeneous and low-loss dielectric multilayer media [recurso eletrônico] / Maria Victoria Africano Contreras. - 2021.

1 recurso online (xviii, 75 f. : il., color.) : pdf.

Orientador: Ricardo Luiz da Silva Adriano.

Coorientador: Diogo Batista de Oliveira

Tese (doutorado) - Universidade Federal de Minas Gerais, Escola de Engenharia.

Bibliografia: f. 66-75.

Exigências do sistema: Adobe Acrobat Reader.

1. Engenharia elétrica - Teses. 2. Antenas (Eletrônica) - Teses. 3. Otimização - Teses. I. Adriano, Ricardo Luiz da Silva. II. Oliveira, Diogo Batista de. III. Universidade Federal de Minas Gerais. Escola de Engenharia. IV. Título.

CDU: 621.3(043)

**"Impulse Ground-penetrating Radar Antenna Design And  
Optimization For Homogeneous And Low-loss Dielectric  
Multilayer Media"**

**Maria Victoria Africano Contreras**

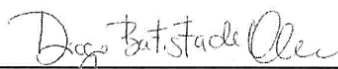
Tese de Doutorado submetida à Banca Examinadora designada pelo Colegiado do Programa de Pós-Graduação em Engenharia Elétrica da Escola de Engenharia da Universidade Federal de Minas Gerais, como requisito para obtenção do grau de Doutor em Engenharia Elétrica.

Aprovada em 14 de abril de 2021.

Por:



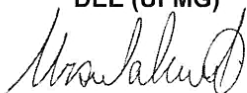
Prof. Dr. Ricardo Luiz da Silva Adriano  
DEE (UFMG) - Orientador



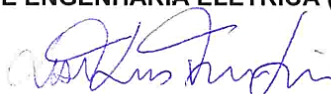
Prof. Dr. Diogo Batista de Oliveira  
DEE (UFMG)



Prof. Dr. Elson José da Silva  
DEE (UFMG)



Prof. Dra. Úrsula do Carmo Resende  
DEPTO DE ENGENHARIA ELETRICA (CEFET -MG)



Prof. Dr. Xisto Lucas Travassos Junior  
Departamento de Engenharias da Mobilidade (UFSC)



Prof. Dr. Fábio Júlio Fonseca Gonçalves  
Campus Ibirité (IFMG)

*To my beloved family*

# Acknowledgments

I would like to express my deep sense of thanks and gratitude to my advisor, Ricardo Adriano, for his pertinent guidance, endless support, patience, and shared knowledge throughout this thesis.

I am also very thankful with my co-advisor, Diogo de Oliveira, for the suggestions and assistance during the development of this research.

I thank profusely to all the lab partners. Especially, to Jose and Poly for their friendship, help, and shared experiences. Also, I want to express my gratefulness to Marlon for being there supporting me, listening to me, and sharing his knowledge and points of view to this thesis.

Special thanks to my dear friend Pilar for her unconditional friendship and all the shared moments. I am also immensely grateful to my dear friend Diego Tami for his constant motivation to accomplish this goal. Thanks for the suggestions and advice.

Finally, I would like to thank the CAPES agency for the financial support given with the scholarship.

# Resumo

A avaliação não destrutiva de meios multicamadas representa um problema eletromagnético inverso que pode ser resolvido com métodos no domínio do tempo ou da frequência, sendo o primeiro mais largamente utilizado. Técnicas de solução no domínio do tempo são populares pois permitem o uso de equações simples e diretas para a obtenção das propriedades das camadas a partir das medições do radar de subsolo (GPR). Para isso são necessárias duas suposições: assume-se que os dielétricos são não magnéticos, de baixa perda e que as camadas são lineares, isotrópicas e homogêneas. Porém, a qualidade dos resultados depende diretamente da correta detecção dos picos de reflexão medidos pelo GPR, o que pode inviabilizar a técnica quando existe sobreposição entre algumas das componentes do sinal recebido pelo GPR.

Nesse contexto, esta tese propôs uma nova metodologia prática para obter os requisitos de projeto da antena (frequência de operação e resposta temporal) que evitem a sobreposição de pulsos refletidos. A metodologia é baseada na análise do sinal de alimentação da antena e na estrutura multicamadas avaliada. A principal contribuição é que a metodologia proposta possibilita a produção de antenas específicas para o problema de multicamadas examinado, servindo como um guia prático para o projeto de antenas GPR. Foi escolhido um pavimento flexível típico composto por três camadas sobrepostas (asfalto, base e subleito) para mostrar como a metodologia pode ser utilizada para obter os requisitos da antena.

Uma vez obtidos os requisitos da antena, topologias candidatas foram selecionadas e duas abordagens de otimização foram propostas e avaliadas: a primeira consiste na otimização no domínio da frequência de um problema multiobjetivo baseado em funções objetivo tradicionais (casamento de impedância e ganho), e a segunda abordagem de otimização utiliza um solucionador eletromagnético no domínio do tempo para avaliar uma nova proposta de função objetivo diretamente no domínio do tempo (a amplitude do pulso recebido).

Como resultado da otimização no domínio da frequência, uma antena monopolo de microfita diretiva e de banda ultralarga (UWB) com dispersão admissível foi obtida

de acordo com as especificações de projeto extraídas do problema de teste. A simulação da antena foi comparada e validada com medições da mesma realizadas em um ambiente não anecoico.

Por sua vez, a otimização da nova função objetivo, aplicada a duas topologias de antenas diferentes (monopolo de microfita e Vivaldi) permitiu obter soluções compactas que atenderam ao requisito da antena no domínio do tempo. Além disso, simulações desse problema de otimização mostraram que a nova função objetivo representa uma alternativa à abordagem de otimização multiobjetivo tradicional. Além disso, a definição de uma única função objetivo facilita o processo de projeto da antena evitando problemas de convergência e qualquer processo posterior de tomada de decisão.

**Palavras-chave:** Radar de subsolo, problema multicamada, pavement materials, ricker wavelet, otimização de antenas UWB.



# Abstract

Non-destructive assessment of multilayer media represents an inverse electromagnetic problem that can be solved with methods in the time- or frequency-domain. Solution techniques in the time-domain are more widely used and popular because they allow the use of simple equations to obtain the layers' properties from the Ground Penetrating Radar (GPR) measurements. For this, it is assumed that the dielectrics are low-loss, non-magnetic, and that the layers are linear, isotropic and homogeneous. However, the quality of the results depends directly on the adequate detection of the reflection peaks measured by the GPR. This can turn the technique unfeasible when there is an overlap between some of the signal components received by the GPR.

In this context, this thesis proposed a new practical methodology to obtain the antenna design requirements (operating frequency and temporal response) that avoid overlapping reflected pulses. The methodology is based on the analysis of the inquiring signal and the evaluated multi-layer structure. The main contribution is that the proposed methodology enables the production of specific antennas for the analyzed multilayer problem, serving as a practical guide for GPR antenna design. A typical flexible pavement composed of three overlapping layers (asphalt, base, and subgrade) was the multilayer structure selected to show how the methodology can be applied to obtain the antenna requirements.

Once the antenna requirements were obtained, the candidate antenna topologies were selected and two optimization approaches were proposed and evaluated: the first one consists of the frequency-domain optimization of a multi-objective problem based on traditional objective functions (impedance matching and gain), and the second optimization approach uses a time-domain electromagnetic solver to assess a new proposal of objective function directly in the time-domain (the received pulse amplitude).

As a result of the frequency-domain optimization, an ultra-wideband (UWB) directive microstrip monopole antenna with admissible dispersion was obtained according to the design specifications extracted from the test problem. The antenna simulation was compared and validated with antenna measurements carried out in a non-anechoic

environment.

In turn, the optimization of the new single-objective function applied to two different antenna topologies (microstrip monopole and Vivaldi) allowed obtaining compact solutions that met the time-domain antenna requirement. Also, simulations of this optimization problem showed that the new objective function represents an alternative to the traditional multi-objective optimization approach. Besides, the definition of one single-objective function facilitates the antenna design process avoiding convergence problems and any posterior decision-making process.

**Palavras-chave:** Ground Penetrating Radar, multilayer problem, pavement materials, ricker wavelet, UWB antenna optimization.

# List of Figures

1.1	Block diagram of a GPR system. . . . .	2
1.2	GPR system given the modulations in the time- or frequency-domain. . . . .	3
2.1	Overlap criterion of Ricker wavelets in time domain. . . . .	13
2.2	Layers model for highways . . . . .	14
3.1	LTI system . . . . .	21
3.2	Link modeling using transfer functions . . . . .	22
3.3	Parametrization of the microstrip monopole antenna with reflector. . . . .	27
3.4	Vivaldi antenna geometry parametrization . . . . .	29
4.1	Final population (blue points) and Pareto front (red points) of the multi-objective problem defined by Eq. (3.1) . . . . .	32
4.2	DE convergence for the optimization problem defined by Eq. (3.2). . . . .	33
4.3	Antenna simulation results. . . . .	35
4.4	Measurement setup. . . . .	36
4.5	Calibration kit ZV-Z135 3.5mm female. . . . .	36
4.6	Designed antenna . . . . .	36
4.7	Photo of the measurement setup. . . . .	36
4.8	S-parameters in dB from HFSS simulation and measurements. . . . .	37
4.9	Realized gain. . . . .	38
4.10	Implemented circuit in ADS . . . . .	39
4.11	Voltage Ricker wavelets at different circuit stages. . . . .	39
4.12	Power pulses in the time-domain . . . . .	40
5.1	Convergence of the single-objective problem for the monopole antenna. . . . .	46
5.2	Boxplot of the monopole antenna variables (left) and best geometry (right) from the last generation. . . . .	47
5.3	Frequency-domain results for monopole antenna from the single-objective problem optimization. . . . .	49

5.4	Pareto fronts of the multi-objective problem (left) and boxplot of the monopole antenna variables (right). . . . .	50
5.5	Frequency-domain results for monopole antenna from the multi-objective problem optimization. . . . .	54
5.6	Convergence of the single-objective problem for the Vivaldi antenna. . . . .	55
5.7	Boxplot of the Vivaldi antenna variables (left) and best geometry (right) from the last generation. . . . .	55
5.8	Frequency-domain results for Vivaldi antenna from the single-objective problem optimization. . . . .	57
5.9	Pareto front of the multi-objective problem (left) and boxplot of the Vivaldi antenna variables (right). . . . .	58
5.10	Frequency-domain results for Vivaldi antenna from the multi-objective problem optimization. . . . .	60

# List of Tables

1.1	UWB-GPR objective functions and types of optimization . . . . .	6
2.1	Estimated values of typical layers' parameters. . . . .	15
2.2	Maximum permissible width for Ricker wavelet per layer. . . . .	15
2.3	Antenna frequency design requirements for the three layer model. . . . .	15
2.4	Complete antenna design requirements for three layer pavement. . . . .	16
3.1	UWB-GPR antennas and characteristics . . . . .	25
3.2	Bound constraints for the monopole antenna. . . . .	28
3.3	Bound constraints for the Vivaldi antenna. . . . .	30
4.1	New monopole antenna parameters obtained from the optimization of the multi-objective problem . . . . .	33
4.2	Signals pulse width. . . . .	40
5.1	New monopole antenna parameters obtained from the optimization of the single-objective problem . . . . .	48
5.2	Time-domain results for monopole antenna from the single-objective problem optimization. . . . .	48
5.3	Time-domain results for monopole antenna from the multi-objective problem optimization. . . . .	51
5.4	New monopole antenna parameters obtained from the optimization of the multi-objective problem . . . . .	52
5.5	Peak values of the received pulse for the best antennas of the multi-objective problem. . . . .	53
5.6	Coefficient of variation of the data on Table 5.5 . . . . .	53
5.7	New Vivaldi antenna parameters obtained from the optimization of the single-objective problem . . . . .	56
5.8	Time-domain results for Vivaldi antenna from the single-objective problem optimization. . . . .	56

5.9	Time-domain results for Vivaldi antenna from the multi-objective problem optimization. . . . .	58
5.10	New Vivaldi antenna parameters obtained from the optimization of the multi-objective problem . . . . .	59

# List of Symbols

$\sigma$	conductivity [ $S/m$ ]
$\omega$	angular frequency [ $rad/s$ ]
$\epsilon$	permittivity
$\sigma$	permeability [ $H/m$ ]
$\mathbf{x}_r(\mathbf{t})$	Ricker wavelet in time-domain
$\mathbf{A}$	amplitude of Ricker wavelet in time-domain
$\tau$	time constant
$\mathbf{t}_0$	time shift
$ \mathbf{X}_r(\mathbf{f}) $	Ricker wavelet amplitude in frequency-domain
$f_p$	peak emission frequency
$t_p$	time-domain pulse width
$d_i$	thickness of layer $i$
$c$	speed of light
$f_C$	central frequency
$f_L$	lower cut-off frequency
$f_H$	higher cut-off frequency
$BW$	bandwidth
$t_{p_{max}}$	maximum time-domain pulse width
$W$	pulse width at half energy
$\epsilon_{r1}$	relative permittivity of medium 1
$\epsilon_{r2}$	relative permittivity of medium 2
$\epsilon_{r3}$	relative permittivity of medium 3
$G$	antenna gain
$G_{mod}$	modified antenna gain
$D$	antenna directivity
$e_{ff}$	antenna efficiency.
$s_r$	received voltage signal in time-domain
$H(\mathbf{w})$	link transfer function
$t_{p_{spread}}$	pulse width with dispersion
$FF$	system fidelity factor
$CV$	Coefficient of variation
$sd$	Standard deviation

# List of Abbreviations

ADS	Advanced design system
ANSI	American National Standards Institute
CEG	correlated energy gain
CPW	Coplanar Waveguide
CST	Computer Simulation Technology
CW-GPR	Continuous-Wave Ground Penetrating Radar
DC	Direct current
DE	Differential evolution algorithm
DOF	Degrees of freedom.
FDTD	Finite-difference time-domain
FFT	Fast fourier transform
GA	Genetic algorithm
GPR	Ground Penetrating Radar
HFSS	High-Frequency Structure Simulator
IEEE	Institute of Electrical and Electronics Engineers
IFFT	Inverse fast fourier transform
LTU	Linear Time-Invariant
NDT	Nondestructive techniques
NSGA-II	Non-dominated sorting genetic algorithm II
PEC	Perfect electric conductor
PSO	Particle Swarm Optimization
s11	Return loss
s21	Transmission coefficient
SPEA2	Strength Pareto Evolutionary Algorithm 2
UWB	Ultra-wideband
VNA	Vector network analyzer
VSWR	Voltage standing wave ratio
XCMP	Extended common mid-point



# Contents

<b>Acknowledgments</b>	<b>vi</b>
<b>Resumo</b>	<b>vii</b>
<b>Abstract</b>	<b>ix</b>
<b>List of Figures</b>	<b>xi</b>
<b>List of Tables</b>	<b>xiii</b>
<b>List of Symbols</b>	<b>xv</b>
<b>List of Abbreviations</b>	<b>xvi</b>
<b>1 Introduction</b>	<b>1</b>
1.1 Objectives and Contributions . . . . .	7
1.2 Survey of chapters . . . . .	8
<b>2 Proposed methodology and test problem definition</b>	<b>9</b>
2.1 Methodology for obtaining antenna requirements . . . . .	9
2.1.1 Inquiring GPR signal . . . . .	9
2.1.2 Impacts of selecting the inverse problem solution approach . . .	10
2.1.3 Pulse overlap criterion . . . . .	12
2.2 Test problem . . . . .	14
<b>3 GPR Antenna optimization</b>	<b>17</b>
3.1 Optimization problem definition . . . . .	18
3.1.1 Multi-objective problem . . . . .	19
3.1.2 Single-objective problem proposal . . . . .	20
3.2 Antenna topology and parametrization . . . . .	23

3.2.1	Parametrization . . . . .	26
3.3	Optimization algorithms . . . . .	30
<b>4</b>	<b>Frequency-domain optimization approach</b>	<b>31</b>
4.1	Antenna multi-objective optimization analysis . . . . .	31
4.2	Simulation of antenna performance . . . . .	33
4.3	Antenna Measurements . . . . .	34
4.3.1	S parameters . . . . .	36
4.3.2	Gain . . . . .	37
4.4	Time domain analysis of the antenna . . . . .	38
4.5	Partial conclusions . . . . .	41
<b>5</b>	<b>Optimization using a time-domain electromagnetic solver</b>	<b>42</b>
5.1	Microstrip monopole antenna . . . . .	45
5.1.1	Single-objective problem . . . . .	45
5.1.2	Multi-objective problem . . . . .	49
5.2	Exponentially tapered slot antenna - Vivaldi . . . . .	54
5.2.1	Single-objective problem . . . . .	54
5.2.2	Multi-objective problem . . . . .	57
5.3	Partial conclusions . . . . .	60
<b>6</b>	<b>Final Considerations</b>	<b>62</b>
6.1	Conclusions . . . . .	62
6.2	List of publications . . . . .	64
6.3	Continuity proposal . . . . .	64
	<b>References</b>	<b>66</b>

# Chapter 1

## Introduction

Nondestructive Testing (NDT) techniques have emerged with the intention of examining any object, material, or system without affecting its future utility. A well-accepted NDT technique is ground penetrating radar (GPR), which has been widely explored and applied in many areas, such as archaeology, geophysics, and engineering [Beben et al., 2013, Van Der Kruk et al., 2007, Huisman et al., 2001]. The GPR technique represents a faster alternative to assess the interior of different structures and also contributes to their preservation.

Several structures, such as railways [Cai et al., 2016], pavements [Fernandes et al., 2017], bedrock and retaining walls [Beben et al., 2013] can be modeled as multilayer media and analyzed using GPR. The GPR has been commonly used as an indirect measurement for the construction and maintenance of highways [Saarenketo and Scullion, 2000]. This topic has been widely explored and a lot of research has been carried out [Spagnolini, 1997, Kurtz et al., 1997, Benedetto and Benedetto, 2002, Colagrande et al., 2011].

For example, [Benedetto and Pensa, 2007] carried out an experimental survey with GPR to calibrate the geophysical parameters and to validate the reliability of an indirect diagnostic method of pavement damage. For the experiments, water was injected into one of the pavement layers for many hours. The experiments proved that it is possible to estimate the volumetric water content in the sub-asphalt layer with a high resolution in space and in time. Another study used GPR to evaluate cover concrete moisture content, commonly used in bridges [Dérobert et al., 2008]. The results showed that GPR was successfully compared during an experimental campaign conducted in the laboratory against several control test slabs. In turn, [Pérez-Gracia et al., 2008] presented various approaches to determine the spatial resolution (SR) in GPR studies. Then, the approach's results were compared with experimental data acquired in both,

a low-attenuating medium and sand.

In broad terms, GPR detects the reflections originating from electromagnetic discontinuities on the structure. Fig. 1.1 presents the block diagram of a GPR system operation. As can be seen, it is composed of transmitter and receiver units, a data processing unit, and finally, a display one. Regarding the antenna system, two main types are commonly used: monostatic and bistatic. Monostatic systems refer to the use of one antenna for transmitting and receiving the signal and bistatic system where two antennas are hosted in the same enclosure, one for transmitting and the other for receiving the signal [Benedetto and Pajewski, 2015].

Basically, GPR sends an electromagnetic signal to the evaluated multilayer surface using a transmitter antenna (Tx). When a material variation, characterized by different electromagnetic parameters, is detected, part of the transmitted energy reflects and the other propagates. This reflected signal is detected by the receiver antenna (Rx), creating a continuous profile of the structure under test while the radar is moving on. All data is shown as a waveform on the display unit and saved for posterior analysis.

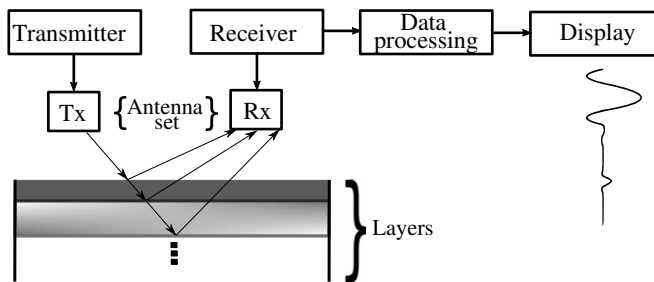


Figure 1.1: Block diagram of a GPR system.

The process of estimate the layer's properties (relative electric permittivity and thickness) from signals acquired with the GPR represents an inverse electromagnetic problem that can be solved using two wide approaches given the waveform used in the GPR: analysis techniques in frequency and time domain [Queiroz et al., 2013]. GPRs that use the energy source in the time-domain are generally known as impulse radars, and the ones that use the source in the frequency-domain and transmit continuously (transmitter always on) are known as CW-GPR. Each GPR type has its advantages and disadvantages. However, most GPR systems use an impulse time-domain waveform and are prevalent in the commercial market because of the simplicity of generating an impulse waveform and low-cost parts [Jol, 2010, p. 74-75]. Besides this, a GPR system can be classified given the employed modulation as shown in Fig. 1.2 [Travassos Jr et al., 2018]. These GPR's modulations are beyond the scope of this

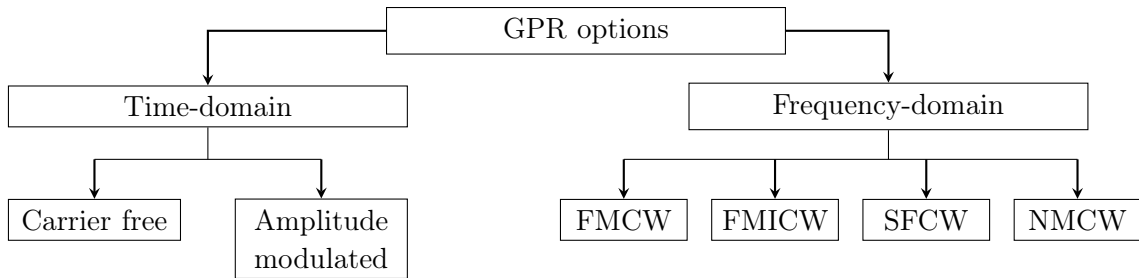


Figure 1.2: GPR system given the modulations in the time- or frequency-domain.

study. For a detailed review on this topic see [Travassos Jr et al., 2018, Jol, 2010].

Choosing a solution technique for the inverse problem has a direct impact on the GPR operating frequency, and, consequently, the antenna to be used. Frequency-domain analysis techniques usually utilize optimization tools to solve the electromagnetic inverse problem [Loulizi et al., 2003, Oliveira et al., 2014]. However, defining the optimization problem based on the reflected electric-field phasor is a challenge, because the uniqueness of the solution must be guaranteed. This means that the objective function must be ensured to have only a unique minimum or maximum point. In a comprehensive study of this problem, Oliveira et al. [Oliveira et al., 2014] presented a methodology that ensures smoothness in the error function of the inverse problem to facilitate its solution. In contrast, the proposed methodology imposes restrictions in GPR center frequency which will limit the minimal size of the antenna. After all, the findings in [Oliveira et al., 2014] suggest working with narrow-band antennas which have analytic closed-form that facilitates its design. Also, many classical narrow-band antennas can be used in this kind of analysis.

In contrast, time-domain analysis techniques generally use the travel time of the electromagnetic wave between the layers and the reflected peak amplitude to define the layers' dielectric properties and thicknesses. However, the quality of results depends on the right detection of the reflection peaks measured by GPR making the technique limited when there is overlap or noise.

For example, a traditional time-domain analysis was proposed in [Loizos and Plati, 2007] and [Lahouar and Al-Qadi, 2008] where the radar pulse propagation (surface reflection) in time is used as the main factor to pavement asphalt layer thicknesses estimation. However, the analysis is performed from visual detection of the received signal which can be affected by specific pavement characteristics. On the other hand, the extended common mid-point (XCMP) method using two air-coupled GPR systems was developed and validated in [Leng and Al-Qadi, 2014] to improve the accuracy of the traditional method for pavement material dielectric

constant estimation. The technique worked better for pavements containing multi-lifts or pavements with non-uniform properties through depth, compared with the classic method based on surface reflection. Nevertheless, the authors affirmed that the performance of the XCOMP method was not as good as the surface reflection method. In a follow-up study, [Zhao and Al-Qadi, 2016] integrated the extended common mid-point (XCOMP) method with stepped-frequency 3-D GPR to obtain asphalt layer thickness. The method presented a low error estimation but for asphalt pavement thinner than 64mm, the 3-D GPR system does not have enough resolution.

To sum up, the traditional time-domain analysis technique uses GPR measurements, easy calculations, and two assumptions to solve the inverse problem: propagation in (a) non-magnetic, low-loss dielectric, i.e., permeability  $\mu_r = 1$  and conductivity  $\sigma \ll \omega\epsilon$ , where  $\omega$  is the angular frequency and  $\epsilon$  is the permittivity; and (b) linear, isotropic and homogeneous layers. Also, it presents a better precision than the other new techniques [Leng and Al-Qadi, 2014]. Therefore, the time domain analysis approach based on travel time through layers presented in [Loizos and Plati, 2007] will be considered for this study from now on. As this technique may become inaccurate if inadequate reflection detections (due to overlapping) are performed, a good vertical resolution is necessary. This means that the transmitted pulse width should not exceed the two-way time that an electromagnetic wave spends traveling during any layer of the evaluated problem. Consequently, there is a need to design antennas with the ability to transmit and receive short pulses with low distortion.

It is believed that the most significant advances in a GPR system can be achieved with the antenna design (transmitter-receiver). In this regard, a complete review of GPR antenna characteristics is presented in [Travassos Jr et al., 2018]. Several studies with specific applications for GPR have been developed to seek antenna systems with optimal design and low-cost [Lestari et al., 2010, Shao et al., 2013, Ahmed et al., 2016]. On this matter, patch antennas have reached increasing prominence by achieving versatile solutions in multiple applications where a radiant element is required [Li and Luk, 2014, Ng et al., 2015, Oliveira et al., 2016].

For instance, authors in [Travassos et al., 2012] proposed using multi-objective optimization to design 3 antennas with applications in 3 different areas, including GPR. In that research, the solution of contradictory objectives related to directivity, impedance matching, cross-polarization, and frequency range using stochastic and deterministic algorithms in the solution was carried out. To find improvements over traditional approaches that only use spectral analysis to optimize antennas, a multi-criteria optimization approach was proposed directly in the time domain [LÁČÍK et al., 2010] for a bow-tie antenna. The results demonstrated a good balance between radiation

and admittance matching in the analyzed frequency range. Besides, another interesting analysis was suggested in [Telzhensky and Leviatan, 2006] to design an optimized antenna that adapts to specific input signals. They ensured a high correlation between the input signal in the time domain and the output signal in the receiving antenna. Further, the authors in [Telzhensky and Leviatan, 2006] achieved not only a minimum Voltage Standing Wave Ratio (VSWR), but also a low temporal dispersion.

Although previous studies have proposed antennas for general GPR applications, none of them is based on the specific problem to establish the antenna-design characteristics, such as the central frequency, bandwidth, and temporal response. Therefore, we propose a practical methodology to obtain the specific antenna-design requirements that allow problems modeled as multilayer media to be solved with the time-domain solution technique while avoiding pulse overlapping. Consequently, the accuracy in the inverse problem solution will be increased due to the design of specific antennas for the problem. In other words, we suggest correlating, in an unequivocal (analytic-direct) way, some *a-priori* physical knowledge of the multilayer problem with the antenna characteristics to be designed. This *a-priori* knowledge means that some typical estimates are known for the relative electric permittivity and thickness of layers, which are generally obtained through other techniques. In this sense, the methodology presented in this thesis represents a practical guide for GPR antenna design, enabling the production of a specific antenna for any analyzed multilayer problem. Consequently, this guide can contribute to obtaining dedicated GPR equipment.

Besides this proposal, another important issue to be established in the GPR optimum antennas design is the definition of the objective problems or goals. It is known that the objective functions should be selected based on the desired antenna characteristics. In this regard, the literature has highlighted several characteristics that the GPR antenna needs to have a good performance [Ali et al., 2017, Travassos Jr et al., 2018, Kundu and Jana, 2018]:

- Wide frequency bandwidth to obtain high resolution,
- good gain and radiation efficiency,
- a good impedance matching,
- low dispersion,
- small size and
- low weight

The design of antenna for applications in GPR is inherently multi-objective given that all these aspects can be defined as objective functions or goals to obtain an optimized GPR antenna. However, they are commonly complex, conflicting, and must be satisfied simultaneously [Travassos Jr et al., 2018]. Up to now, a considerable amount

of literature has been published on UWB-GPR antenna optimization. Regarding the definition of objective functions and the selected optimization type (parametric or topology), some references were summarized in Table 1.1.

Table 1.1: UWB-GPR objective functions and types of optimization

Ref.	Objective functions and optimization type	
<sup>a</sup>	Two multi-objective optimization types for UWB antenna design were presented. The first type was based on parametric optimization where the three proposed goals were: the summation of the magnitude of the reflection coefficient raised to cube, the standard deviation of the peak gain, both obtained at nine frequencies varying from 3GHz to 10.6GHz, and the summation of the fidelity factors obtained at different sampled directions. The second type was based on topology optimization defining as goals: the summation of the magnitude of the reflection coefficient raised to cube, the standard deviation of the broadside antenna gain, and the standard deviation of the group delay. These goals were obtained from 3GHz to 11GHz at steps of 0.25GHz.	
<sup>b</sup>	A weighted cost function was proposed for the parametric optimization of UWB monopole and dipole antenna using a genetic algorithm (GA). The cost function correlates the least matched magnitude in the s11 parameter and the average of the fidelity factor measured at different positions.	
<sup>c</sup>	The cost function defined for the parametric optimization was the weighted sum of two functions: the first one was the maximum value of VSWR in the UWB band, and the second one was a function based on the average correlation factor simulated at three different positions.	
<sup>d</sup>	Three parameters were proposed for parametric optimization: the reflection coefficient, the fidelity factor, and the cross-polarization level. The multi-objective optimization was performed using the Particle Swarm Optimization (PSO) and an antipodal Vivaldi antenna for UWB applications.	
<sup>e</sup>	The objective function selected for the parametric optimization was the fidelity of the time-domain response of a UWB thin-wire bow-tie dipole antenna for GPR applications.	
<sup>f</sup>	The fitness function defined for the parametric optimization was to maximize the sum of the time-domain fidelity and the inverse of the VSWR referenced to 250Ω to design a bow-tie antenna with central frequency at 255MHz for UWB short pulse GPR applications.	
<sup>g</sup>	The parametric optimization involved three objectives: the reflection response, the average total efficiency in 3.1GHz to 10.6GHz range, and the size, of three different UWB antenna geometries.	
<sup>h</sup>	A parametric optimization with three objectives was proposed to design a UWB antenna to work in the frequency range between 0.5 GHz and 3 GHz: s11 bandwidth, gain bandwidth, and gain in the broadside direction.	
<sup>i</sup>	The cost function selected was the mean effective correlated energy gain using parametric time-domain optimization.	
<sup>a</sup> [Chen, 2016]	<sup>b</sup> [Dumoulin et al., 2012]	<sup>c</sup> [Chamaani and Mirtaheeri, 2010]
<sup>d</sup> [Chamaani et al., 2011]		<sup>e</sup> [Van Coevorden et al., 2006]
<sup>f</sup> [Faraji et al., 2009]		<sup>g</sup> [Koziel and Bekasiewicz, 2017]
<sup>h</sup> [Moreno de Jong van Coevorden et al., 2013]		<sup>i</sup> [Xie et al., 2011]

From Table 1.1, it is possible to observe that the authors have tended to focus on multi-objective problems rather than on single-objective ones. Also, it can be stated



that different objectives have been used to design UWB-GPR antennas and that there is no consensus among the authors about the way of satisfying all the objectives at the same time. Nevertheless, some of them are more commonly used. For instance, the impedance matching, represented by the VSWR or the  $s_{11}$  parameter, is almost always selected for UWB antenna optimization because it is used to adjust the antenna bandwidth. Besides, this parameter is frequently optimized along with the antenna gain or efficiency to maximize its value or to maintain it constant in the desired frequency band.

Selecting multiple objectives will increase the complexity of finding solutions and, consequently, the computational cost. Therefore, the weighted sum method was used by some authors as a strategy to deal with the multi-objective problems (See Table 1.1). The general idea of this method is to associate a weight to each objective function and to minimize the weighted sum of the goals. In this way, the multi-objective problem is transformed into a single- or mono-objective problem [Marler and Arora, 2010]. This allows correlating somehow the variables. Nevertheless, the weights are empirically selected by the authors.

The findings in the literature motivated the study of the multi-objective problem based on traditional approaches and the proposal of a new single quality metric to align several of the antenna characteristics.

## 1.1 Objectives and Contributions

This work aims to design an optimal antenna set to be used in GPR systems dedicated to multilayer problems. To achieve this goal, the following steps were carried out:

- To develop a methodology that allows obtaining the spectral and temporal antenna characteristics based on a specific multilayer problem.
- To validate the proposed methodology applying it to a pavement problem.
- To select a candidate antenna topology, based on the spectral and temporal requirements obtained from the methodology and the pavement problem.
- To define the optimization problem so that the selected antenna topology meets the spectral and temporal antenna requirements.
- To validate the antenna design by comparing antenna measurements and simulations.

One contribution of this thesis is the proposal of a new practical methodology to obtain the antenna design requirements (operating frequency and temporal response) from the analysis of the assessed multilayer problem. This proposal allows avoiding the issue of overlapping reflected pulses presented in impulse GPR applications. The main finding is that the proposed methodology enables the production of specific antennas for the analyzed homogeneous and low-loss dielectric multilayer problem, serving as a practical guide for GPR antenna design.

Another contribution is the proposal of a single quality metric for antenna design that intends to align the desired antenna characteristics to obtain a better time-domain antenna response. Also, the definition of one single-objective problem can facilitate the antenna design process avoiding convergence problems and any posterior decision-making process. This single metric can be applied to all directive UWB antenna designs, not just those for GPR.

Overall, we believe that this work has a significant contribution because represents an alternative for obtaining low-cost GPR equipment with higher precision in layers estimation. Besides, low-cost antennas with minimized volumes can be built, allowing to obtain a more compact GPR system. Partial results of this thesis were published in the *Journal of Microwaves, Optoelectronics and Electromagnetic Applications (JMoe)* [Africano et al., 2020].

## 1.2 Survey of chapters

This thesis is organized into six chapters as follows: Chapter 2 presents the step-by-step formulation to obtain the frequency requirements for the antenna design in section 2.1. Then, section 2.2 contains a description of a simple multilayer medium used to test the methodology proposed in section 2.1. Later, Chapter 3 explains the UWB antenna selection and defines the developed optimization problems to fulfill the requirements obtained for the test problem of section 2.2.

Chapter 4 addresses the results of the frequency-domain optimization approach to solve a multi-objective problem applied to a monopole antenna with a reflector. In this chapter, the optimized antenna was validated through simulations and measurements.

Then, Chapter 5 presents the results of an optimization approach using a time-domain electromagnetic solver. The new single-objective proposal and a traditional multi-objective problem were evaluated for two antenna topologies, a monopole antenna with a reflector and a Vivaldi antenna. Finally, Chapter 6 shows the conclusions of this thesis, the list of publications, and the continuity proposal.

# Chapter 2

## Proposed methodology and test problem definition

### 2.1 Methodology for obtaining antenna requirements

As was pointed out in the introduction, the antenna design is dependent on the GPR operating frequency, which in turn depends on the type of analyzed multilayer structure and the inquiring signal. From this correlation, the following methodology was developed. The methodology starts with the analysis of the inquiring GPR signal. Then, some information from the time-domain inverse problem solution is extracted, and finally, a signal-overlap criterion is established according to [Jol, 2010, p. 15]. Following these methodology steps, the requirements for antenna design can be obtained for a specific multilayer problem. Thus, if an antenna meets those requirements, the overlapping reflected pulses would be avoided. In this way, the proposed methodology serves as a practical guide in the design of GPR antennas.

#### 2.1.1 Inquiring GPR signal

There are different kind of pulses that are commonly used in GPR applications. The most widely studied pulse is the Gaussian along with its respective derivatives [Uduwawala, 2007, Lin et al., 2008, Kumar and Maiti, 2014]. The Ricker wavelet corresponds to the second derivative of the Gaussian pulse. It is frequently used in GPR applications [Zhao et al., 2015, Nobes, 2017] because it solves the problem of low-frequency components (spectrum near to DC) presented in the Gaussian pulse.

Therefore, the Ricker wavelet is the pulse selected for use in the proposed methodology.

The equation that describes Ricker wavelet is as follows:

$$x_r(t) = A \left[ 1 - \frac{2}{\tau^2}(t - t_0)^2 \right] \exp \left\{ -\frac{(t - t_0)^2}{\tau^2} \right\} \quad (2.1)$$

where  $A$  is the amplitude,  $t_0$  is the time shift, and  $\tau$  is the time constant.

The Fourier transform amplitude  $|X_r(f)|$  of the Ricker wavelet is given in Eq. (2.2).

$$|X_r(f)| = A(2\pi f)^2 \exp \left\{ -\frac{1}{4}(2\pi f\tau)^2 \right\} \quad (2.2)$$

The peak emission frequency  $f_p$  can be found deriving Eq. (2.2) and equaling to zero.

$$\frac{d|X_r(f)|}{df} = 2A\pi^2 f [4 - (2\pi f\tau)^2] \exp \left\{ -\frac{1}{4}(2\pi f\tau)^2 \right\} \quad (2.3)$$

As a consequence, the peak emission frequency should satisfy  $(2\pi f\tau)^2 = 4$ . By isolating  $f_p$  from this term and assuming that the pulse width is  $t_p \approx 6\tau$ , Eq. (2.4) is obtained.

$$f_p = \frac{6}{\pi t_p} \quad (2.4)$$

As shown, it is possible to define, through Ricker wavelet analysis, the peak emission frequency  $f_p$ . This frequency represents the antenna's central frequency, which is an important parameter in the antenna design. As can be seen in Eq. (2.4), the pulse width  $t_p$  is still an unknown variable which will be obtained in the next methodology step.

### 2.1.2 Impacts of selecting the inverse problem solution approach

Selecting an approach (either in the time or frequency-domain) to solve the inverse problem imposes a set of restrictions leading to different GPR operating frequencies. The time-domain analysis approach uses a short pulse to feed the GPR antenna, which results in a spectrum rich in frequency components. The pulse width in this technique is determined by the analyzed multilayer structure.

In the time-domain analysis approach, an adequate identification of each reflected pulse is necessary because the layers' characteristics, such as thickness and permittivity, are obtained from the time between multiple pulse reflections and their amplitudes. A complete description of the approach can be found in [Loizos and Plati, 2007, Africano, 2015]. In this way, the total time of the incident pulse for each interface should be less than the time for the transmitted wave portion to travel through the next layer, reflect on the next interface, and return.

The intersection of subsequent pulses will be null if:

$$t_p \leq 2\Delta t d_i, \quad \forall_i = 0, 1, \dots, n. \quad (2.5)$$

where  $t_p$  is the Ricker wavelet width, Let  $\Delta t d_i$  represents the required time for the wave to travel through layer  $d_i$ , and  $n$  is the number of layers in the problem. The time that the pulse takes to travel through each layer ( $\Delta t d_i$ ) is obtained by:

$$\Delta t d_i = \frac{d_i \sqrt{\epsilon_i}}{c} \quad (2.6)$$

where  $\epsilon_i$  and  $d_i$  are the relative electric permittivity and thickness of layer  $i$ , respectively and  $c$  is the speed of light. Thus, by substituting Eq. (2.6) in Eq. (2.5), the general equation for any multilayer problem is obtained:

$$t_p \leq 2 \left( \frac{d_i \sqrt{\epsilon_i}}{c} \right), \quad \forall_i = 0, 1, \dots, n. \quad (2.7)$$

It is evident, from Eq. (2.7), that both the thinnest layer thickness and the lowest permittivity determine the selection of  $t_p$ . In this way, the pulse width is defined in terms of relative electric permittivity and thickness of each layer using some a-priori knowledge about the analyzed structure, as will be explained in the next section.

Now, the appropriate spectral requirements for designing the antenna from the analyzed multilayer structure can be completely defined. First, the peak emission frequency  $f_p$  can be calculated using Eq. (2.4) where  $t_p$  is a pulse width satisfying (2.7). Then, the cut-off frequencies and bandwidth can be defined for  $f_p$ . These frequencies are commonly selected depending on the application. For instance, ANSI STD C63.10-2013 [ANSI, 2013] and IEEE STD 686-2017 [IEEE, 2017] define for UWB and radar devices respectively that the cut-off frequencies  $f_L$  and  $f_H$  are the lowest and highest frequencies where the signal is at least 10 dB below the peak power level. On the other hand, circuit theory commonly defines these frequencies when the peak power

falls at half (-3dB) [Boylestad and Nashelsky, 2013]. For this work, the half-width cut-off frequencies at -6 dB were used because it allows a pulse reconstruction closer to the Ricker wavelet. Thus, the approximations for the frequency-domain parameters of the Ricker wavelet as a function of  $f_p$ , as determined by Wang in [Wang, 2015], are as follows:

$$f_C \approx 1.059095f_p \quad (2.8)$$

$$f_L \approx 0.481623f_p \quad (2.9)$$

$$f_H \approx 1.636567f_p \quad (2.10)$$

$$BW \approx 1.154944f_p \quad (2.11)$$

where  $f_C$  is the central frequency,  $f_L$  and  $f_H$  are the lower and upper cut-off frequencies, respectively and  $BW$  is the bandwidth. These specifications guarantee that there will not be any pulse overlap which contributes to the accuracy of the solution technique of a GPR inverse multilayer problem. In summary, the antenna to be used in GPR equipment must be capable of transmitting a Ricker wavelet respecting the characteristics described by Eqs. (2.4) and (2.8)-(2.11).

### 2.1.3 Pulse overlap criterion

The spectral and temporal antenna characteristics were already obtained in sections 2.1.1 and 2.1.2. Nevertheless, antennas are inherently dispersive elements and, therefore, can cause undesired reflections. It is important to know which is the antenna's permissible dispersion ( $t_{pmax}$ ) that still allows separating the reflections originated from multilayer discontinuities. For this, the criterion proposed by Jol [Jol, 2010, p. 15] for a Gaussian pulse was used and adapted for Ricker wavelet.

Fig. 2.1 shows the extremes for two Ricker wavelets, in which the pulse is characterized by the width at half energy  $W$  defined by the time difference between the extremes of pulse when they achieve half of the maximum value of energy. Fig. 2.1(a) depicts pulses that are clearly separable without any overlap. In turn, Fig. 2.1(b) presents pulses that overlap but are still considered distinguishable (separable). According to [Jol, 2010, p. 15], two Gaussian pulses are distinguishable if they are separated by at least the width at half amplitude, as shown in Fig. 2.1

Therefore, if certain pulses are allowed to overlap by the width at half energy  $T \approx W$ , the restriction of the pulse can now be given by:

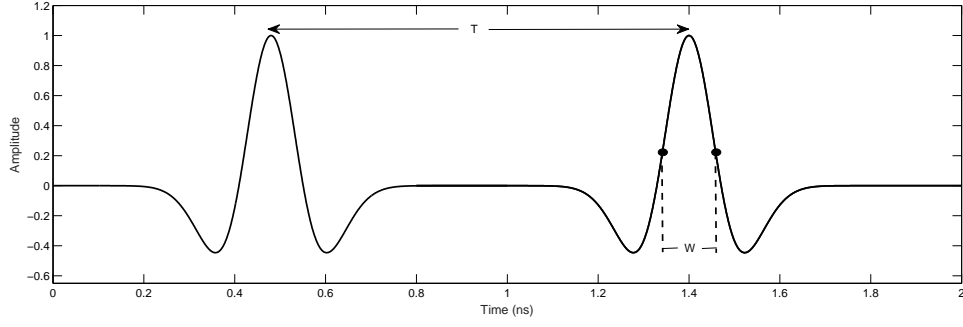
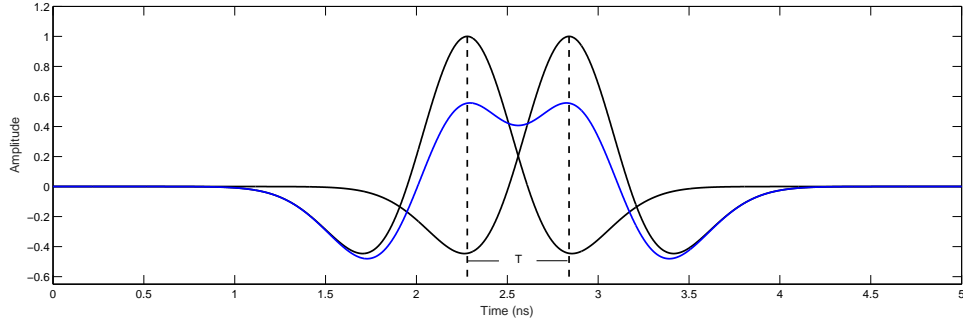
(a) Clearly separated ( $T \gg W$ )(b) Still distinguishable  $T \approx W$ 

Figure 2.1: Overlap criterion of Ricker wavelets in time domain.

$$W \leq 2\Delta t d_i, \quad \forall_i = 0, 1, \dots, n. \quad (2.12)$$

where

$$W \approx \frac{t_{p_{max}}}{5}. \quad (2.13)$$

By substituting Eq. (2.13) in (2.12) and using Eq. (2.6), the allowed maximum pulse width ( $t_{p_{max}}$ ) is given by:

$$t_{p_{max}} \leq 10 \left( \frac{d_i \sqrt{\epsilon_i}}{c} \right), \quad \forall_i = 0, 1, \dots, n. \quad (2.14)$$

As a result, the dispersive characteristic of the antenna is defined from the separation threshold between two pulses.

Thus, given an estimate of the multilayer problem to be assessed, the design antenna requirements can be defined using Eqs. (2.8)-(2.11) and (2.14), as will be presented next.

## 2.2 Test problem

A multi-layer structure was selected in this work to show how the proposed methodology can be used. GPR has been used commonly as an indirect measurement for construction and maintenance of highways [Saarenketo and Scullion, 2000], where pavement can be modeled by multiple overlapping layers. This topic has been widely explored and much research has been carried out, such as [Benedetto and Benedetto, 2002], [Colagrande et al., 2011].

The three-homogeneous-layer model presented in Fig. 2.2 was used as a test pavement problem. A bistatic antenna system was picked and we assumed that the two antennas on the test link can point to the target in the direction of maximum radiation. In Fig. 2.2, Tx and Rx represent the transmitter and receiver antennas, respectively,  $d_0$  is the distance between the pavement surface and the antennas.  $d_1$  and  $d_2$  are the unknown layer thicknesses,  $\epsilon_{r1}$ ,  $\epsilon_{r2}$  and  $\epsilon_{r3}$  are the unknown relative electric permittivities related to each layer (1 for asphalt, 2 for base and 3 for sub-grade layer).

To apply the methodology described previously, the first step is to calculate the Ricker wavelet width by using Eq. (2.7). This equation is dependent on  $\epsilon_{r_i}$  and  $d_i$ , which are unknown parameters (they are predicted with GPR testing). Then, some a-priori knowledge of the range of possible values of the electromagnetic properties and thicknesses of the pavement layers needs to be considered here. This interval can be defined using some direct measurements in the tested multilayer media using destructive techniques or it can also be defined using the results of typical pavement values of permittivities and thicknesses, which were measured or estimated in previous works [Saarenketo and Scullion, 2000, Maharaj and Leyland, 2010, Hidalgo et al., 2010]. To the test problem proposed in this work, the range of the permittivity and thickness of each layer are shown in Table 2.1 [Saarenketo and Scullion, 2000, Maharaj and Leyland, 2010, Hidalgo et al., 2010].

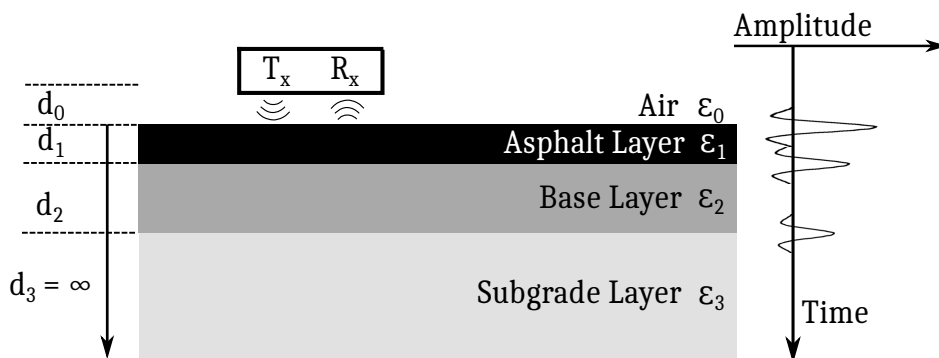


Figure 2.2: Layers model for highways



Table 2.1: Estimated values of typical layers' parameters.

Layer	$\epsilon_r$	$d_i$ (cm)
1. Asphalt	3 - 12	6 - 10
2. Base	5 - 10	20 - 30
3. Sub-grade	10 - 25	—

Table 2.2: Maximum permissible width for Ricker wavelet per layer.

Layer	$\epsilon_{r_{\min}}$	$d_{\min}$ (cm)	$t_p$ (ns)
0. Air	1	15	1
1. Asphalt	3	6	0,69
2. Base	5	20	2,98

Table 2.3: Antenna frequency design requirements for the three layer model.

Parameter	Value (GHz)
$f_p$	2.77
$f_c$	2.93
$f_L$	1.33
$f_H$	4.53
$BW$	3.2

The most restrictive case was selected from Table 2.1 to generate a worst-case analysis. This means that the smallest values of both permittivity and thickness of each layer in Table 2.1 were used to calculate  $t_p$ , and, from these  $t_p$  values, the shortest travel time was selected. In this way, the non-overlap in the GPR reflected pulses will be ensured, regardless of the real value of the pavement parameters. Thereby, the pulse width of Ricker wavelet was calculated for each layer using Eq. (2.7), and the obtained values are listed in Table 2.2.

It can be defined from the data in Table 2.2 that if the pulse width is at most 0.69 ns, the overlap between layers reflections for the pavement problem would be avoided. Thus, it is demonstrated that the pulse was actually defined based on *a-priori* pavement physical knowledge assuming a worst-case scenario.

The next step of the proposed methodology is to calculate the peak emission frequency  $f_p$  using Eq. (2.4) where the  $t_p$  is the one obtained for the thinnest layer in Table 2.2 ( $t_p = 0.69$ ns). Then, the antenna design values were calculated using Eqs. (2.8) - (2.11). Thus, all the spectral antenna requirements were estimated; they are presented in Table 2.3.

Finally, the maximum antenna permissible dispersion was calculated for the thinnest layer (asphalt) using Eq. (2.14). The result indicates that a maximum width

Table 2.4: Complete antenna design requirements for three layer pavement.

Parameter	Value
$t_p$	0.69 ns
$f_C$	3 GHz
$f_L$	1.5 GHz
$f_H$	4.5 GHz
$BW$	3 GHz
$t_{p_{max}}$	3.4 ns

of Ricker wavelet  $t_{p_{max}} \leq 3.46\text{ns}$  would still allow to separate reflections from each layer.

So far, the specific spectral and temporal requirements for antenna design were obtained using the methodology proposed in section 2.1 given the pavement in Fig. 2.2. These requirements were all approximated as presented in Table 2.4.

The chapter that follows moves on to consider the process to obtain a new antenna that attends to the requirements.

# Chapter 3

## GPR Antenna optimization

Optimization is a process widely studied in many fields like mathematics, statistics, economics and computer science. Optimization methods use algorithms and models from mathematics, statistics and evolution theory in the attempt to find the minimum or maximum value of a function, known as objective function, under certain constraints [Africano, 2015].

The UWB antenna design literature shows two types of antenna optimization that have been widely explored: parametric and topology optimization [Kundu et al., 2018, Ahmed et al., 2016, Koziel and Bekasiewicz, 2017, Liu et al., 2014, Chen and Chiu, 2016]. In broad terms, parametric optimization refers to the adjustment of a set of antenna variables whose topology was previously chosen. These parameters are related with geometric characteristics such as dimensions of microstrip line, patch and ground plane. In this way, the parametric optimization guarantees certain properties inherited from characteristics of the initial antenna topology.

On the other hand, topology optimization constructs the antenna structure by varying the material distribution within the design domain providing a large-scale of degrees of freedom (DoF) [Chen and Chiu, 2016, Travassos Jr et al., 2018]. Besides, [Liu et al., 2014] affirms that the optimized antenna using topology optimization can be obtained within a shorter time with less trial and error than using parametric optimization. However, the irradiation mechanism of the optimized antenna is not well known and sensitivity analysis and robustness test must be introduced in the optimization process to minimize the influence of the manufacturing uncertainties [Travassos Jr et al., 2018].

Most of the research on this topic has focused in parametric optimization. For instance, a microgenetic algorithm was applied in [Van Coevorden et al., 2006] to design a UWB thin-wire bow-tie antenna with broadband characteristics (achieved by

resistive loading). In the study, a parametric optimization was conducted by selecting the geometry of the antenna as well as the values of the resistors located along the structure. The initial antenna topology was optimized to find an adequate design for the detection of fractures in a marble quarry. In another similar study, a multi-objective optimization algorithm was used to find the optimum curved parameters of a resistively loaded Wire-bow antenna [Faraji et al., 2009]. The analyzed parameters were resistive loads along the antenna arms, load's locations, number of wires and the angular distances between wires. Results of the study showed a significant performance improvement in comparison with previous bow-tie antennas. Another parametric optimization was performed in [Lee et al., 2005] to design a CPW-fed antenna for UWB applications. The geometric parameters were obtained using CST Microwave Studio based on the finite-integration method.

Regarding UWB antenna topology optimization, [Chen and Chiu, 2016] applied the Strength Pareto Evolutionary Algorithm 2 (SPEA2) to obtain the optimum pixelated layout of the surface in designing a UWB planar monopole antenna. The results of the study showed the capability of the optimization method and they demonstrated that the antenna fulfilled the established requirements. [Liu et al., 2014] proposed a miniature antenna design method of planar bow-tie antennas using topology optimization with the method of moving asymptotes. It was shown in the results of the study that the center operating frequency of the antenna was reduced significantly but a diminution in bandwidth and gain was evidenced. [Hassan et al., 2014] carried out gradient-based topology optimization for the design of metallic antennas. For this, they suggested variations of the distribution of material conductivity in a given domain to design the radiating patch of both planar monopole antennas and microstrip antennas. The obtained geometries presented arbitrary unknown shapes because there were no prior assumptions about details in the designs.

Admittedly, both types of optimization have interesting aspects to be separately explored in the optimization process. But throughout this thesis, parametric optimization was preferred because the obtained antennas would be easier to construct with the available laboratory tools and materials.

### 3.1 Optimization problem definition

In GPR context, it is desirable to design an antenna with the maximum energy projected to the surface (directional), robust, mobile, with input impedance transformed to  $50 \Omega$  to minimize losses caused by decoupling between the antenna and the radar.

To achieve these characteristics the following approaches were specified.

### 3.1.1 Multi-objective problem

As stated in the introduction of this thesis, most researches have selected different objective functions, being the most typical, the impedance matching and gain. Therefore, two optimization problems were defined based on these characteristics.

1. Initially, gain and impedance matching were proposed as goal functions for antenna optimization. In this way, we have:

$$\begin{aligned} \text{minimize } f_o(x) &= \begin{bmatrix} \max_f \text{VSWR}(f, \mathbf{x}) \\ -G(\mathbf{x}) \end{bmatrix} \\ \mathbf{x}_{\min} &\leq \mathbf{x} \leq \mathbf{x}_{\max} \end{aligned} \quad (3.1)$$

2. Then, the impedance matching was prioritized as goal function being the optimization problem stated as:

$$\begin{aligned} \text{minimize } f_o(x) &= [\max_f \text{VSWR}(f, \mathbf{x})] \\ \mathbf{x}_{\min} &\leq \mathbf{x} \leq \mathbf{x}_{\max} \end{aligned} \quad (3.2)$$

In Eqs. 3.1 and 3.2,  $\mathbf{x}$  is the solution vector containing the geometry parameters presented in previous section,  $VSWR$  is the Voltage Standing Wave Ratio of the antenna as function of  $\mathbf{x}$  and the frequency band  $f$  obtained for the test problem described in section 2.2.  $G$  represents the antenna gain and the vectors  $\mathbf{x}_{\min}$  and  $\mathbf{x}_{\max}$  are the minimum and maximum values of each geometry parameter.

As can be seen in Eqs. 3.1 and 3.2, a minimum VSWR value is desired because it represents how well the antenna is matched. If this value is equal to one means that there would no be reflected voltage. Consequently, antenna designs always search for a VSWR lower than 2 which means that, approximately, 10 % or less of the voltage is reflected. On the other hand, a high gain is desirable. Therefore, the objective function 1 ( $f_{o1}$ ) defines the worst VSWR value found in the analyzed bandwidth and the objective function 2 ( $f_{o2}$ ) represents the negative gain at center frequency evaluated in the region of interest.

### 3.1.2 Single-objective problem proposal

The definition of this single-objective problem was motivated by two facts:

1. The difficult convergence characteristic of the multi-objective problems given the complex objectives and the need of being satisfied simultaneously.
2. The gain and impedance matching defined as goals does not directly attend to the requirement of low distortion of the received signal which as stated before is one of the most important GPR antenna characteristics to be guaranteed.

Therefore, the new objective function proposed in this work for GPR antenna design is the maximization of the received pulse amplitude. By increasing the amount of energy in the region of interest, the gain, the signal phase, and the impedance matching in the frequency band should present good performance. Otherwise, the signal amplitude would decrease. Consequently, this proposal allows aligning and weighting the common goals using only one objective function.

The single-objective problem can then be defined as:

$$\begin{aligned} \text{minimize } f_o(x) &= -(\max |s_r(t, \mathbf{x})|) \\ \mathbf{x}_{\min} &\leq \mathbf{x} \leq \mathbf{x}_{\max} \end{aligned} \quad (3.3)$$

where,  $\mathbf{x}$  is the solution vector containing the geometry parameters,  $s_r$  represents the received voltage signal by the antenna in time domain and  $\mathbf{x}_{\min}$  and  $\mathbf{x}_{\max}$  are the bound constraints.

The antenna optimization defining a single metric in the time-domain is rarely addressed in the literature. A study in this area is the work of [Xie et al., 2011] where the proposal is to optimize the correlated energy gain (CEG) presented as  $G_C$  in Eq. 3.4.

$$G_C(\theta, \phi) = \frac{1}{\eta_0} \frac{\left[ \int_{-\infty}^{+\infty} \mathbf{E}(t, R, \theta, \phi) \cdot \mathbf{a}(\theta, \phi) v_s(t) R dt \right]^2}{\int_{-\infty}^{+\infty} |v_s(t)|^2 dt} \quad (3.4)$$

where  $\eta_0$  is the intrinsic impedance of free space,  $\mathbf{E}(t, R, \theta, \phi)$  is the time-domain radiated electric field at the position  $(R, \theta, \phi)$ ,  $\mathbf{a}(\theta, \phi)$  is the unit vector expressing the desired polarization of the antenna, and  $v_s(t)$  is the incident voltage in the feeding line of the antenna.

According to the author, "the CEG takes into account the effects of the mismatching, the waveform distortion, the antenna efficiency, and the directivity. Thus it

is a good descriptor to estimate the time-domain performance of the UWB antenna." However, the proposed objective function (CEG) performs an integral of the time-domain radiated electric field, leading to disregard the pulse width. Besides, CEG in [Xie et al., 2011] was not applied to directive antennas which is a primary aim of GPR applications. Therefore, the optimization problem proposed in this thesis and given by the Eq. (3.3) is more appropriate than the CEG in [Xie et al., 2011] for GPR applications because our proposal prioritizes the energy concentration leading to have lower pulse dispersion.

It is now necessary to explain how to obtain the received antenna signal ( $s_r$ ) defined as objective problem. For this, it is well-known that the radiated field or output response of a two-antenna system can be predicted by using transfer functions [Qing et al., 2006, Elmansouri et al., 2012].

- **Antenna transfer function**

A UWB link can be described as a Linear Time-Invariant (LTI) system as shown in Fig. 3.1 where the output signal in the frequency ( $S_t$ ) or time domain ( $s_r$ ) is obtained by the product or convolution of the input signal with the transfer function.

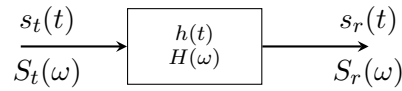


Figure 3.1: LTI system

The transmission parameter  $s_{21}$  is equivalent to the system transfer function but a time-consuming link simulation should be done to calculate it for a limited distance of separation. As an alternative, [Quintero et al., 2011] defined in detail the following formulation to obtain the impulse response of the system using simulations from one single antenna. The system frequency domain equations were preferred, because most antenna characteristics are in the frequency domain, as same as most equipment [Quintero et al., 2011]. We will use the term  $H(\omega)$  to refer to the system transfer function hereafter.

The transfer function in Fig. 3.1 can be extended to represent the complete UWB link which is composed by the transmitter antenna, the propagation channel and the receptor antenna as shown in Fig. 3.2. Therefore, the transfer function of the complete system is defined by Eq. 3.5.

$$H(\omega) = \frac{S_t(\omega)}{S_r(\omega)} = H_{Tx}(\omega)H_{Ch}(\omega)H_{Rx}(\omega) \quad (3.5)$$

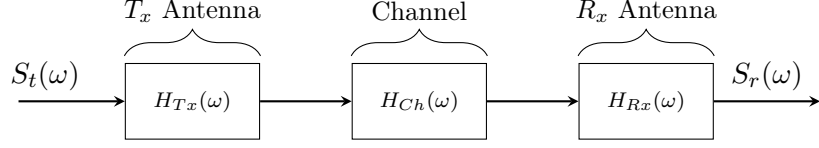


Figure 3.2: Link modeling using transfer functions

The voltages ratio between the received signal in  $R_x$  and the transmitted signal at the input in  $T_x$  can be defined using Friis equation:

$$\frac{P_{R_x}}{P_{T_x}} = e_{pol} (1 - |\Gamma_{T_x}|^2) (1 - |\Gamma_{R_x}|^2) G_{T_x} G_{R_x} \left( \frac{\lambda}{4\pi r} \right)^2 \quad (3.6)$$

where  $e_{pol}$  is the polarization efficiency of the system,  $\Gamma$  is the reflection coefficient which represents the mismatch at each antenna terminal, and  $G$  is the total antenna gain. The last term represents the free-space loss factor where  $\lambda$  is the wavelength and  $r$  is the antenna distance.

Assuming that there is no polarization loss because the antennas are located at the same plane and assuming two equal antennas, it can be defined that  $e_{pol} = 1$ ,  $G_{T_x} = G_{R_x}$  and  $\Gamma_{T_x} = \Gamma_{R_x} = s_{11}$ . Then, the gain and the reflection coefficient can be obtained from the simulation of a single antenna.

Finally, the power ratio can be expressed as voltages ratio knowing that  $P_{R_x} = V_{R_x}^2 / Z_{R_x}$  and that the impedance of the transmitter and receiver antenna are the same. Thus, the expression of the transfer function amplitude is given by:

$$|H(\omega)| = \left| \frac{V_{R_x}}{V_{T_x}} \right| = (1 - |s_{11}|^2) G \frac{\lambda}{4\pi r} \quad (3.7)$$

To estimate the phase of  $H(\omega)$ , the phase distortion inside the antennas is calculated using the phase of the radiated electric field given by simulations, and the phase of the channel is obtained from the well-known function  $e^{-jkr}$ . In this way, we have:

$$\angle H(\omega) = -\phi_{T_x} - kr + \phi_{R_x} \quad (3.8)$$

In [Quintero et al., 2011], after some manipulations Eqs. (3.7) and (3.8) are separated in order to have the three transfer functions  $H_{T_x}$ ,  $H_{Ch}$ , and  $H_{R_x}$ . Then, we have:



$$H_{Ch} = \frac{\lambda}{4\pi r} e^{-jkr} \quad (3.9)$$

$$H_{Tx} = \sqrt{\frac{2\pi c(1 - |s_{11}|^2)G}{\omega}} e^{j\phi_{Rx}} \quad (3.10)$$

$$H_{Rx} = \sqrt{\frac{\omega(1 - |s_{11}|^2)G}{2\pi c}} e^{j\phi_{Rx}} e^{-j\frac{\pi}{2}} \quad (3.11)$$

- **Time-domain received signal**

Once the transfer functions of the antennas and the channel are expressed, the time-domain signal at the output of the system can be obtained. As we already know the input pulse in the time-domain and its characteristics, a fast Fourier transform (FFT) provides the frequency spectrum of that pulse. Then, it is multiplied by the transfer function and the frequency-domain received signal can be obtained (Eq. (3.12)). Finally, an inverse fast Fourier transform (IFFT) allows obtaining the received signal in the time-domain (Eq. (3.13)).

$$S_R(\omega) = H(\omega) FFT(s_t(t)) \quad (3.12)$$

$$s_R(t) = IFFT(S_R(\omega)) \quad (3.13)$$

## 3.2 Antenna topology and parametrization

In the impulse GPR system, an extremely short pulse is transmitted and the frequency spectrum of this signal has a bandwidth of several GHz. Consequently, the UWB antenna characteristic must be ensured. In this regard, the IEEE Standard for Radar Definitions [IEEE, 2017] has defined that a radar is UWB if the fractional bandwidth,  $B_F$ , expressed in Eq. (3.14), exceeds 0.25.

$$B_F = \frac{BW}{f_C} = 2 \frac{f_H - f_L}{f_H + f_L} \quad (3.14)$$

where  $BW$  is the bandwidth defined as  $f_H - f_L$ ,  $f_C$  is the center frequency of the band given by  $(f_L + f_H)/2$ , and  $f_H$  and  $f_L$  are the upper and lower limits of the band, respectively.

As previously stated for parametric optimization, an initial antenna topology that adapts to the specific application should be defined. The GPR pavement problem described in section 2.2 requires that the antenna present high electromagnetic performance, low cost and low profile [Travassos Jr et al., 2018]. Particularly, microstrip patch antennas have been widely used because they are small, and can be designed to work at different frequencies and polarization. Also, they have low implementation cost [Oliveira et al., 2016]. On the other hand, microstrip patch antennas have some drawbacks that can be minimized, such as: low efficiency, limited power and narrow band characteristics.

In broad terms, the microstrip patch antennas are an extension of the microstrip transmission lines. They have a small (comparable with  $\lambda$ ) metallic patch located on a dielectric substrate characterized by  $\epsilon_r$ , which is in turn located on a ground plane. The canonical forms, such as rectangle, square, circle, triangle, among others, are generally used to design the patch. This antenna type was selected to perform all the analysis throughout this thesis.

Many topologies of UWB-GPR antennas have been proposed and studied in the literature that could meet the requirements obtained in chapter 2.2: bowtie antennas [Zhao et al., 2014, Yang, JianKishk, 2011], spiral slot antennas [Omar et al., 2013], circular antennas [Karim et al., 2013], Vivaldi antennas [Arezoomand et al., 2017], resistive linear antennas [Kim and Scott, Jr., 2004], among others [Travassos Jr et al., 2018]. Some specific antenna topologies were analyzed and its main characteristics consigned in Table 3.1.

In this thesis, the selected antenna geometry was inspired in the microstrip monopole antenna shown in [Kasi and Chakrabarty, 2012]. It represented a good starting point since it has a simple geometry for construction and parametrization, light weight, and low profile. In general terms, the microstrip monopole antennas have a geometry very similar to the microstrip patch antennas. Therefore, designers commonly use the design equations of the patch antenna presented in [Balanis, 2016, p. 788-792] as a basis of a sensibility analysis or optimization process. The main difference between the microstrip monopole and patch antenna is that the former has a modification of the ground plane (some parts are removed) which allows widening the impedance bandwidth. This antenna topology has been widely explored in literature for different applications and many modifications have been tested and validated, such as [Chamaani and Mirtaheri, 2010, Kundu and Jana, 2018, Khan et al., 2018, Karoui et al., 2019]. The reported monopole antennas have been designed to cover the 3.1–10.6 GHz unlicensed UWB band and the gains present variations between 2 and 5 dB.

Table 3.1: UWB-GPR antennas and characteristics

Ref.	Antenna	Size (mm <sup>3</sup> )	Gain (dB)	Bandwidth (GHz)	Substrate permittivity
a	Bow-tie with reflector	40x70x1	Stable at 9.5	1.97-6.49	2.65
b	Self-grounded bow-tie	54x58x24	5-8	2-15	–
c	Spiral slot	61x61x0.38	2-6	3.1-10.6	9.5
d	Slotted microstrip patch	90.5x45.3x1.57	max. 10.5	1.91-2.51	2.2
e	Circular patch with reflector	200x250x1.57	6.2-6.8	0.5-2	2.2
f	UWB antipodal Vivaldi	250x134x0.75	7-14	2-18	3
g	Vivaldi with metamaterials	140x80x0.5	9-14	2.5-13.5	2.65
h	Resistive Linear	171.5x114.3x–	0-5	2.8-10	3.4
i	U-shaped rectangular patch	40x35x1.57	3-6	3.6-12	3
j	Elliptic	21x27x1.6	max. 6	3.1-19	4.4
k	Double circular ring	26x22x1.6	2.4 dB at 3 GHz	3.1-16	4.4
a	[Zhao et al., 2014]	b	[Yang, JianKishk, 2011]	c	[Omar et al., 2013]
d	[Islam et al., 2008]	e	[Karim et al., 2013]	f	[Orrillo et al., 2010]
g	[Zhou and Cui, 2011]	h	[Kim and Scott, Jr., 2004]	i	[Kasi and Chakrabarty, 2012]
j	[Karoui et al., 2019]	k	[Khan et al., 2018]		

Specifically, the antenna in [Kasi and Chakrabarty, 2012] is composed of a radiator with a U-shaped rectangular patch combined with a transition step fed by a microstrip line and a partial ground plane. It has a gain that varies from 3 to 6 dB and the bandwidth from 3.6 to 12 GHz, which means that it is not in the desired frequency band. Besides, it has an omnidirectional radiation pattern. To solve this, a reflector plane was added behind the antenna and a parametric optimization was carried out. The inclusion of the reflector plane will allow the antenna to be directive. However, it will make impedance matching more challenging.

Another antenna geometry was also selected to be optimized: the exponentially tapered slot antenna, commonly called Vivaldi. This geometry was chosen because there is a large number of published studies in GPR applications (e.g. [Liu and Sato, 2014, Elsheakh and Abdallah, 2019, Guo et al., 2019, Sun et al., 2021]) that highlight its characteristics, such as wide bandwidth, featured directive radiation, planar structure, easy fabrication [Bhattacharjee et al., 2020]. In literature, there are many variations of the initial geometry (proposed in [Gibson, 1979]) to enhance the antenna performance. Nevertheless, one of the limitations found in the Vivaldi antenna design is that researchers have not explained in detail the selection of the antenna parameters, such design is empirical. Some formulations are usually defined to estimate a few antenna parameters, but they are adjusted then through simulations. Therefore, it is difficult to define the limits of the search space and adapt them to the desired requirements.

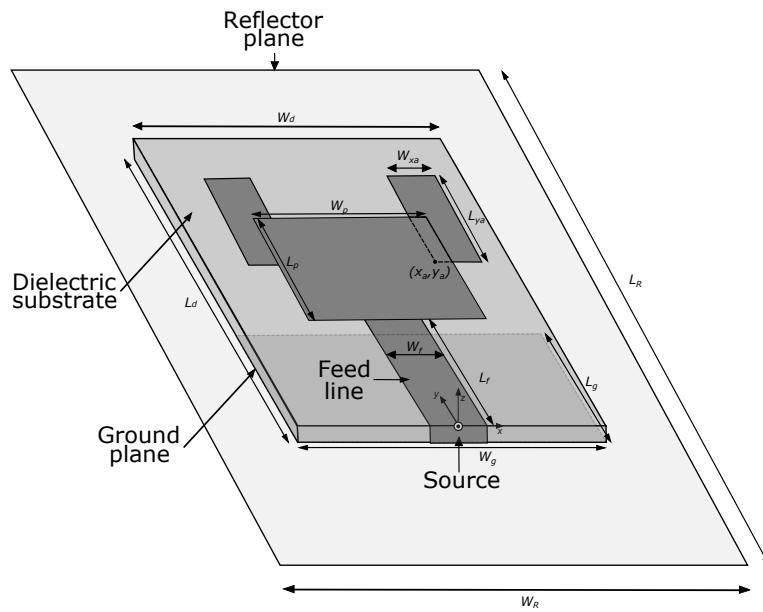
Vivaldi antennas reported in the literature, considering different geometry modifications and substrate materials, have presented excellent bandwidths extending up to approximately 18 GHz. The gains present variations between 1.5 and 13 dB.

The specific antenna geometry approached in this thesis is shown in [Balanis, 2016, p. 497]. A modification in the microstrip transmission line was performed to improve the field matching in the transmission line. In general terms, the Vivaldi antenna in [Balanis, 2016] is fed via the microstrip to slot line transition. The microstrip line is located in the bottom cladding of the dielectric substrate and the uniform slot is connected to the exponentially tapered slot in the upper face of the substrate.

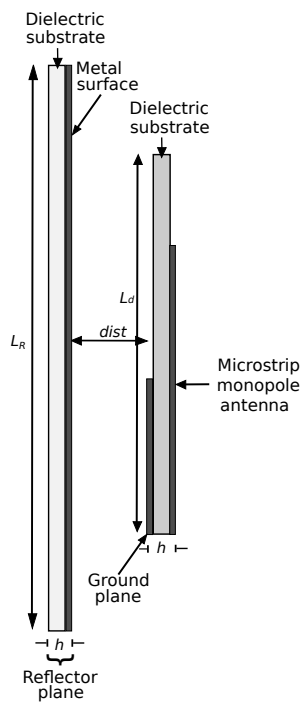
### 3.2.1 Parametrization

Fig. 3.3 shows the geometry of the microstrip monopole antenna with reflector (hereafter referred to as monopole antenna) where fifteen parameters were used to describe it: the width  $W_d$  and length  $L_d$  of the dielectric substrate, the width  $W_f$  and the length  $L_f$  of the feed line, the width  $W_p$  and the length  $L_p$  of the patch, the width  $W_g$  and the length  $L_g$  of the ground plane, the position on the x- and y-axis of one of the arms  $(x_a, y_a)$ , the width  $W_{x_a}$  and the length  $L_{y_a}$  of the arm. To reduce the search space, the dimensions of the other arm were obtained assuming that the antenna is symmetrical. Finally, the width  $W_R$  and the length  $L_R$  of the reflector plane as also the distance  $D_R$  between the reflector plane and the antenna. The dielectric substrate thickness was defined as constant ( $h=1.6\text{mm}$ ).

The limits of the monopole antenna variables taken as bound constraints for the



(a) Perspective view



(b) Cross-section view

Figure 3.3: Parametrization of the microstrip monopole antenna with reflector.

optimization problems are presented in Table 3.2.

Interestingly, although the proposed parametrization was based on the one in [Kasi and Chakrabarty, 2012], it covers a much larger search space. This is because there is no imposition for the antenna arms to be connected to the central patch. In

Table 3.2: Bound constraints for the monopole antenna.

$x_{\min}$ (mm)	Variable	$x_{\max}$ (mm)
40	$W_d$	80
35	$L_d$	80
1	$W_f$	15.1
5.3	$L_f$	48
8	$W_p$	64
0.48	$L_p$	74.8
20	$W_g$	80
4.7	$L_g$	80
3	$x_a$	24
8.6	$y_a$	78.4
0.48	$W_{xa}$	37
0.028	$L_{ya}$	71.4
8.4	$dist$	25.1

this way, the parametrization can describe monopole antennas with parasitic elements or even monopoles with slots, commonly used for impedance matching. Then, the proposed parametrization expands the search space but, at the same time, it returns a more challenging process in the solution search.

The Vivaldi antenna geometry and its parametrization is presented in Fig. 3.4 where nine parameters were used to describe it: the length  $L_{taper}$  of the exponential ground radiator, the width  $W_d$  of the dielectric substrate, the width  $s$  and the length  $L_s$  of the slot, the length  $L_a$  of the back-wall offset rectangle, the distance  $W_{pos}$  from  $y=0$  to the  $45^\circ$  wedge, the width  $W_m$  and the length  $Q_{wm}$  of the transmission line, and finally, the exponential rate of the ground radiator  $Rate$ . The dielectric substrate thickness was defined as constant ( $h=1.5\text{mm}$ ). The exponential ground radiator given the initial  $(x_1, y_1)$  and final  $(x_2, y_2)$  points is calculated using Eq. (3.15) [Yang et al., 2008].

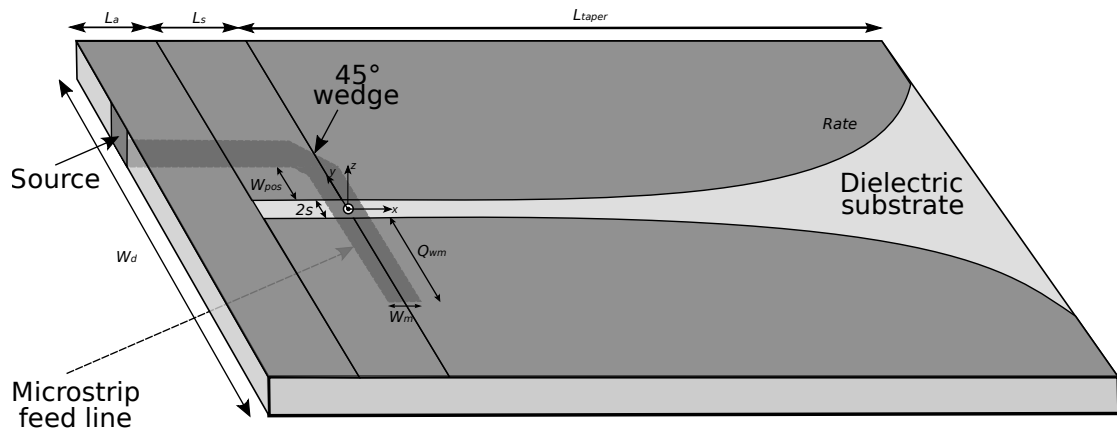
$$y(x) = C_1 e^{Rate \cdot x} + C_2 \quad (3.15)$$

where

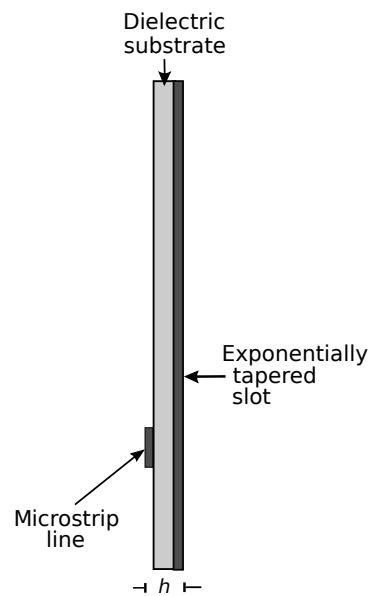
$$C_1 = \frac{y_2 - y_1}{e^{Rate \cdot x_2} - e^{Rate \cdot x_1}} \quad (3.16)$$

$$C_2 = \frac{y_1 e^{Rate \cdot x_2} - y_2 e^{Rate \cdot x_1}}{e^{Rate \cdot x_2} - e^{Rate \cdot x_1}} \quad (3.17)$$

It is stated in [Balanis, 2016, p. 497] that the directivity of Vivaldi antennas increases as the length ( $L_{taper}$ ) of the antenna increases. On the other hand, the



(a) Perspective view



(b) Cross-section view

Figure 3.4: Vivaldi antenna geometry parametrization

bandwidth is limited by the opening width  $W_{min}$  ( $2s$ ) and the aperture width of the antenna (controlled by the exponential rate). Also, it is affirmed that the optimal antenna performance is achieved when the length  $L_{taper}$  is greater than one wavelength at the lowest frequency. However, evaluating an antenna of 200 mm represents a high computational cost which is not desirable when handling many geometries. Therefore, restrictions were imposed on this value to reduce the computational cost and, also, to get a compact antenna geometry.

The limits of the Vivaldi antenna variables taken as bound constraints for the optimization problems are presented in Table 3.2.

Table 3.3: Bound constraints for the Vivaldi antenna.

$x_{\min}$ (mm)	Variable	$x_{\max}$ (mm)
70	$L_{taper}$	140
70	$W_d$	140
0.5	$s$	3
4	$L_s$	25
0.5	$L_a$	3
0.5	$W_{pos}$	66
2	$W_m$	5
1	$Q_{wm}$	10
50	$Rate$	200
0	$RateN$	1

### 3.3 Optimization algorithms

Two algorithms were selected to solve the optimization problems defined in section 3.1: the Differential Evolution (DE) algorithm and the Non-dominated Sorting Genetic Algorithm (NSGA-II). Both were adapted and ran in MATLAB following the references [Price et al., 2006, Deb et al., 2002]. These algorithms were employed as tools to evaluate the objective functions and compare them. Therefore, they were not finely syntonized to the problem because a sensitivity analysis of the control parameters implies a high computational cost. Thus, the control parameters chosen for the search of the optimal set were the default values proposed by the authors [Price et al., 2006, Deb et al., 2002].



# Chapter 4

## Frequency-domain optimization approach

This chapter presents the results of the optimization process using the commercial software High-Frequency Structure Simulator (HFSS) to compute the electromagnetic quantities defined as objective functions in the Eqs. (3.1) and (3.2). Thus, MATLAB and HFSS were used together through Visual Basic scripting (VB script). In this way, MATLAB compiles the sequential DE algorithm with population size  $N_{pop} = 30$  and number of generations  $gen = 100$ , where the last parameter was the only stop criterion. The setting of DE operators was 0.8 and 0.6 for crossover and mutation, respectively.

HFSS is a frequency domain electromagnetic solver based on the finite element method. Setting a fine frequency sweep in the band will increase the computational time for each solution, which is not desirable when handling many geometries. Therefore, the gain was calculated in the central frequency and only five frequencies were established in the HFSS frequency sweep to make the optimization process faster when calculating the  $s_{11}$  parameter.

### 4.1 Antenna multi-objective optimization analysis

1. The first optimization problem consisted of minimizing both, the negative gain at the central frequency and the worst VSWR value of the band (Eq. (3.1)). Fig. 4.1 presents the obtained solutions by the implemented algorithm. As can be observed, the solutions presented good gain values (the lowest around 5 dB) but none of the VSWR values is less than 2 in the desired frequency band. The stopping criteria was achieved (100 generations) and the solutions did not satisfy the VSWR requirements.

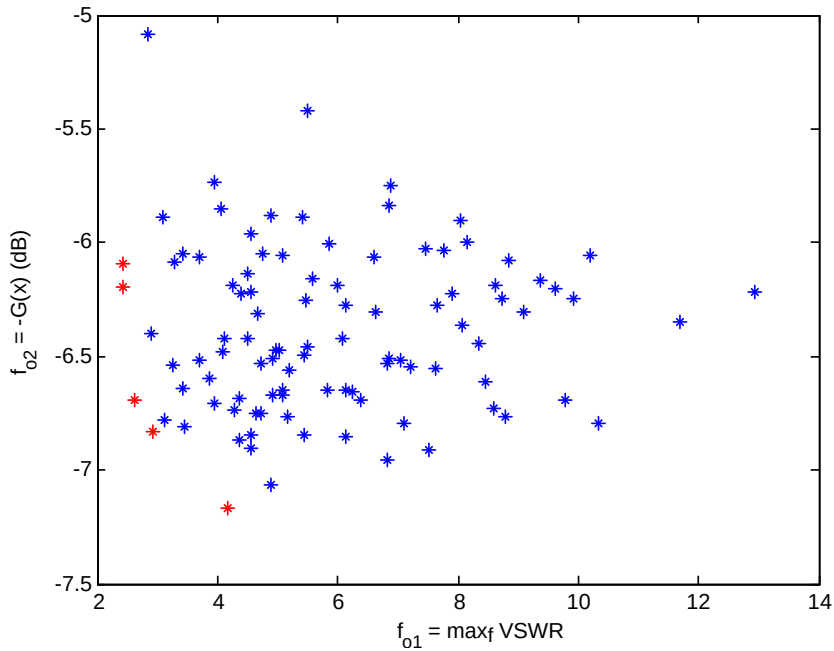


Figure 4.1: Final population (blue points) and Pareto front (red points) of the multi-objective problem defined by Eq. (3.1)

In summary, these results indicate that the defined multi-objective problem is of difficult convergence making the algorithm incapable to find the optimal solution. Besides, the time the algorithm spent obtaining the solutions on Fig. 4.1 was approximately four weeks, which means that the optimization of this problem is computationally expensive, even assuming only five frequency points to calculate each objective function.

2. As a consequence of the multi-objective problem results, the second optimization problem was defined prioritizing the VSWR as showed in Eq. (3.2). The convergence results of this problem are depicted in Fig. 4.2. The dashed red line represents the desired maximum VSWR threshold for the frequency band. As shown in Fig. 4.2, VSWR values that meet the specified requirement were found. Subsequently, a gain sensitivity analysis was performed because very low gain values could be found. Thus, the gain values for the optimized antennas were collected and compared with each other setting the minimum acceptable gain to 2 dB. After this procedure, the best antenna geometry was obtained and its parameters are shown in Table 4.1.

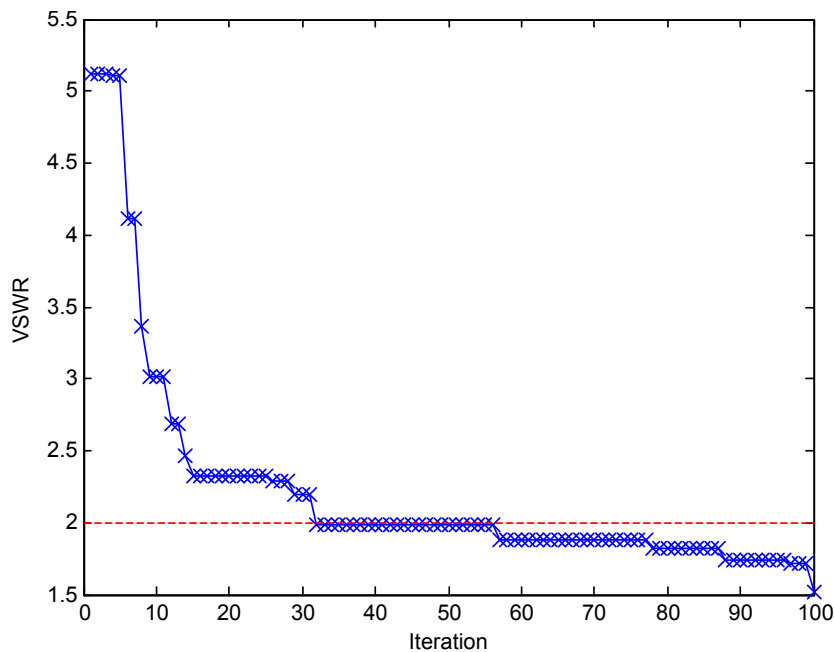


Figure 4.2: DE convergence for the optimization problem defined by Eq. (3.2).

Table 4.1: New monopole antenna parameters obtained from the optimization of the multi-objective problem

Parameter	Value (mm)
$W_d$	47.9
$L_d$	78.5
$W_f$	2.54
$L_f$	28.5
$W_p$	13.3
$L_p$	35.3
$W_g$	35
$L_g$	25.3
$x_a$	6.99
$y_a$	31.2
$W_{xa}$	16.9
$L_{ya}$	24.4
$W_R$	90
$L_R$	120
$dist$	22.5

## 4.2 Simulation of antenna performance

The antenna topology shown in Fig. 3.3 was simulated in HFSS using a fine frequency sweep and the parameters in Table 4.1. The microstrip line, patch, arms, ground, and reflector plane were modeled as perfect electric conductors (PECs), and a port was

connected to the microstrip line as the feed. The PEC elements were all placed in an FR4 low-cost substrate considering  $\epsilon_r = 4.4$ , and  $\tan\delta = 0.02$ .

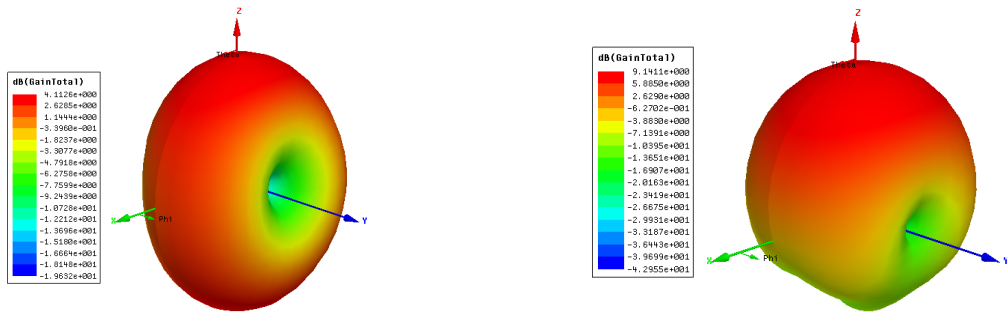
In order to show how the antenna characteristics are affected by the presence of the reflector plane, the new antenna was simulated and analyzed with the reflector plane and without it (see Fig 4.3).

The 3D radiation pattern simulated in the central operating frequency (3GHz) for the antenna is presented in Fig. 4.3(a). It can be observed from Fig. 4.3(a) that the designed antenna has an omni-directional radiation pattern, as expected from the initial topology. Figs. 4.3(b) and 4.3(d) show that the inclusion of the reflector plane made the radiation pattern directive not only at central frequency but in the complete bandwidth. On the other hand, the VSWR presented an increase at low frequencies of the analyzed band (see Fig. 4.3(c)). However, this does not represent a drawback, since the most important antenna parameter to be guaranteed in the GPR inverse problem solution technique is the pulse fidelity rather than the power transmission.

### 4.3 Antenna Measurements

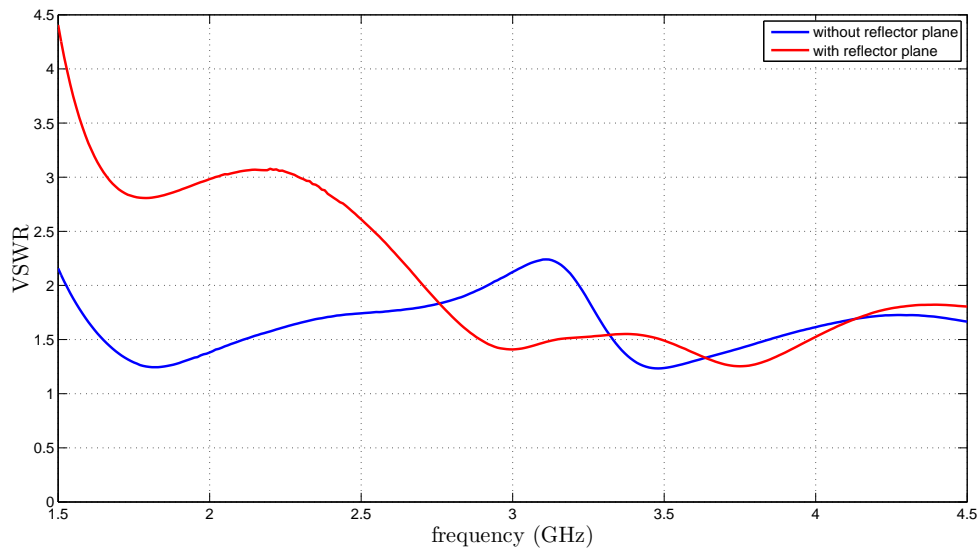
A Rohde & Schwarz vector network analyzer (VNA) with coaxial testing cables was used in a non-anechoic environment to perform the measurements, as represented in Fig. 4.4. The coaxial cables were properly calibrated using the thru-open-short-match (TOSM) calibration and the ZV-Z135 3.5mm female calibration kit from Rohde and Schwarz (Fig. 4.5). Finally, the antennas were connected to the coaxial cables using female SMA -  $50\Omega$  connectors. Both antennas were aligned, facing each other in the boresight direction.

The antenna was built in a  $47.9 \times 78.5 \times 1.6 \text{ mm}^3$  FR-4 low-cost substrate and it is shown in Fig. 4.6. The transmitter-receiver link measurements were performed placing two equal antennas separated a distance considered of far-field ( $5\lambda$  of the operating central frequency) in a non-anechoic environment, taking one hundred measurements of each parameter. Fig. 4.7 presents the photo of the measurement setup inside the laboratory. The antenna holding structure was handcrafted where two sets of an antenna and a reflector plane were fixed on two separate polystyrene pieces using cut skewer sticks. The employed measurement methodology was improved and presented in [Artur et al., 2017]. At the same time, this link was modeled in HFSS for antenna validation, which comprises comparing the measured results of gain, and transmission losses with the simulated ones.

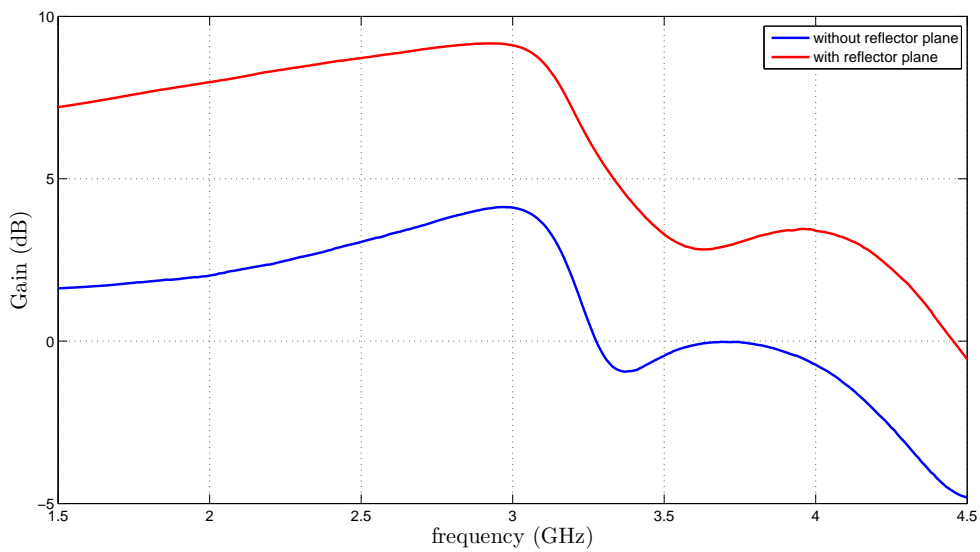


(a) Total gain without reflector plane

(b) Total gain with reflector plane



(c) VSWR



(d) Total gain

Figure 4.3: Antenna simulation results.

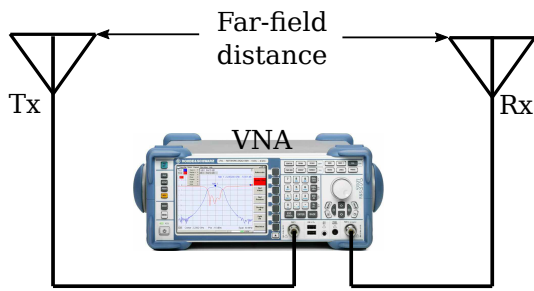
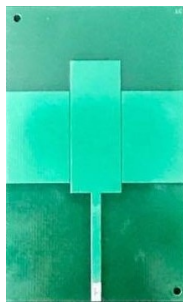


Figure 4.4: Measurement setup.



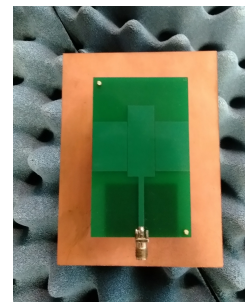
Figure 4.5: Calibration kit ZV-Z135 3.5mm female.



(a) Front view



(b) Back view



(c) Front view with reflector plane

Figure 4.6: Designed antenna

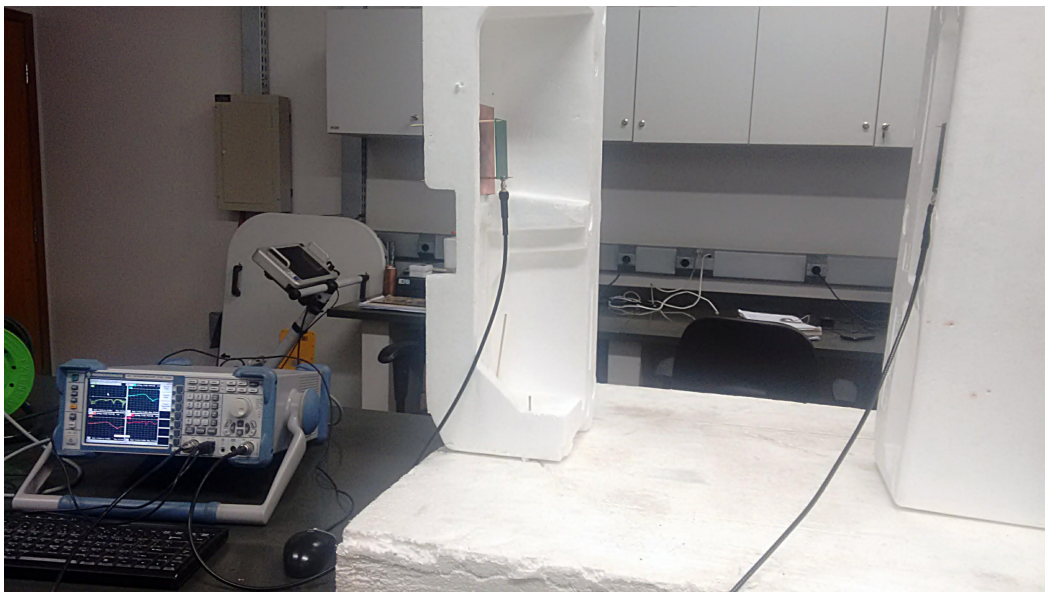


Figure 4.7: Photo of the measurement setup.

### 4.3.1 S parameters

The S parameters from the antenna measurement were exported and compared with the simulation ones (see Fig. 4.8). It is observed from Fig. 4.8 that the results present a good correlation at frequencies higher than 3 GHz. It can also be seen that the reflection

coefficient ( $s_{11}$ ) is better in measurements within the whole bandwidth. This indicates that the reflection losses are negligible and less than 10% of the voltage energy returns to the source. Differences in the measured and simulated values presented in Fig. 4.8 may be due to the non-anechoic environment, uncertainties in the FR-4 electromagnetic properties, and mechanical inaccuracies in the positioning of the antennas and the reflector plane.

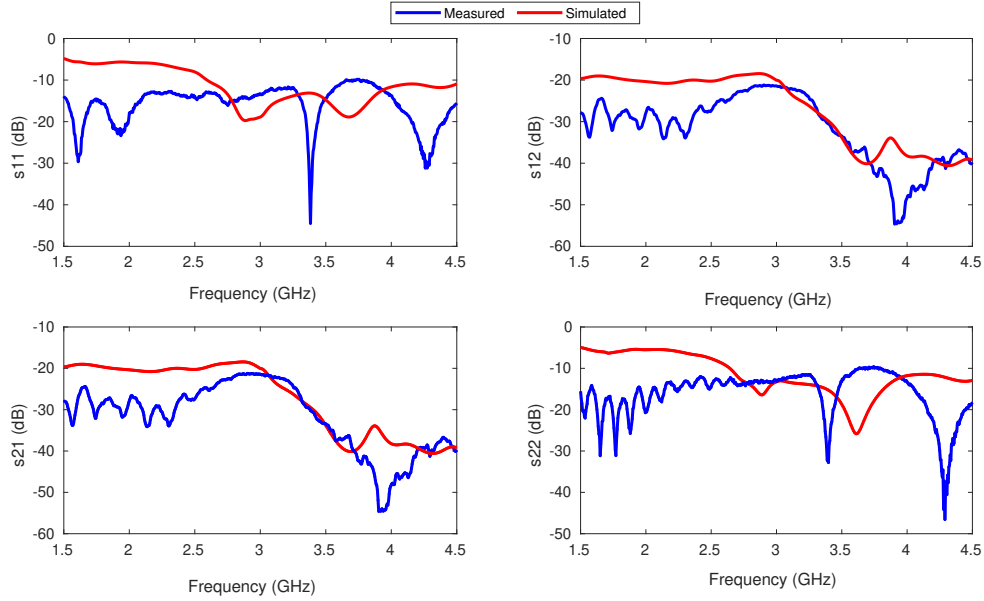


Figure 4.8: S-parameters in dB from HFSS simulation and measurements.

### 4.3.2 Gain

Friis transmission equation was used as shown in Eq. (4.1) to calculate the antenna realized gain where  $r$  is the distance between two equivalently designed antennas,  $\lambda$  is the free-space wavelength and  $s_{21}$  is the transmission coefficient.

$$G = \frac{4\pi r}{\lambda} |s_{21}| \quad (4.1)$$

Fig. 4.9 shows the gains calculated using Eq. (4.1) from the HFSS simulated link (red line) and the measured link (blue line), comparing them with the HFSS gain for a single antenna (black). This comparison was performed as a validation of the Friis approximation where the distance between the antennas must be far-field. Thereby, Fig. 4.9 illustrates that the defined Friis approximation using the distance of 50 cm provides good results comparing the red and black lines.

In contrast, gain from the measurements was satisfactory at frequencies higher than 3GHz. However, the results differ from simulated ones at lower frequencies. This result was expected because Friis equation depends on  $s_{21}$  parameter, which has a similar behavior between simulated and measured results (see Fig. 4.8).

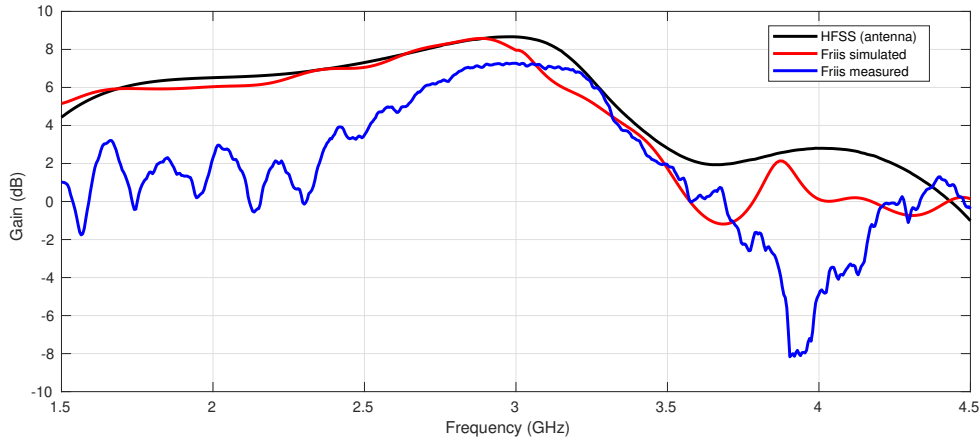


Figure 4.9: Realized gain.

## 4.4 Time domain analysis of the antenna

A pulse temporal analysis was performed using the designed antenna to visualize the signal spread. To achieve this, the S-parameters were exported from HFSS and from measurements to the Advanced Design System (ADS) software, where they are modeled as a two-port black box. Fig. 4.10 shows the complete simulated circuit of a Ricker wavelet transmission and reception using the designed antenna. The only change between measured and simulated pulses is the black box containing the S-parameters. The Ricker wavelet was imported to ADS from MATLAB with a pulse width  $t_p = 0.69$  ns and connected to a  $50\text{-}\Omega$  resistance.

The voltage signal at each node (1-Transmitted, 2-Coupled, 3-Received in Fig. 4.10) was simulated and the results are presented in Fig. 4.11. In Fig. 4.11, small reverberations in the signal coupled to the antennas (black line) can be seen. These are due to impedance matching, and therefore, existing reflections are added to the input signal (red line). The blue line in Fig. 4.11 represents the output signal which was multiplied by a factor (of 50) for visualization purposes.

To perform the spread (dispersion) analysis, the power at the system output (node 3 in Fig. 4.10) was analyzed. A shorter spread time indicates that there will be no overlap of reflected signals, which is desirable. The simulated and measured



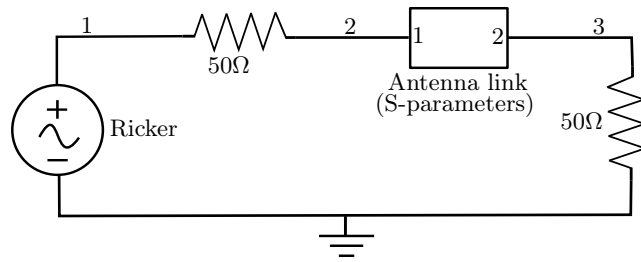
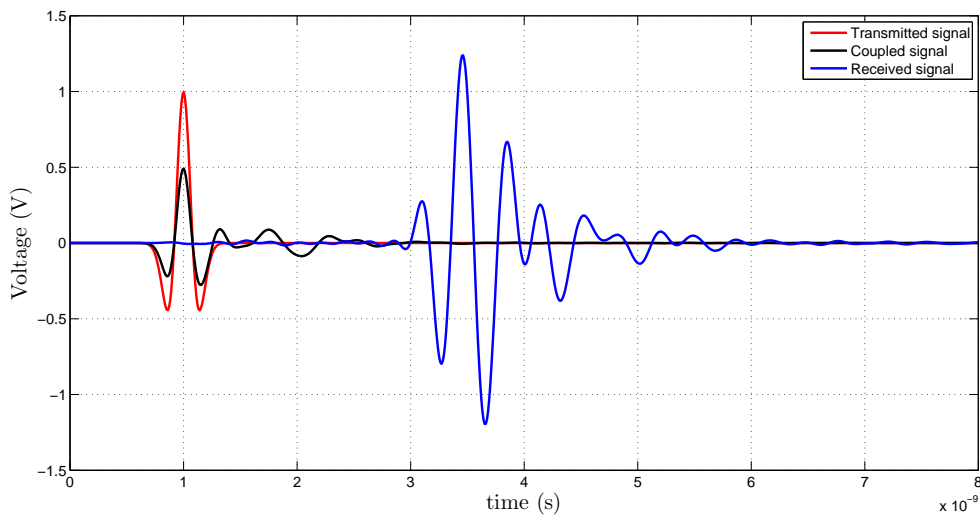
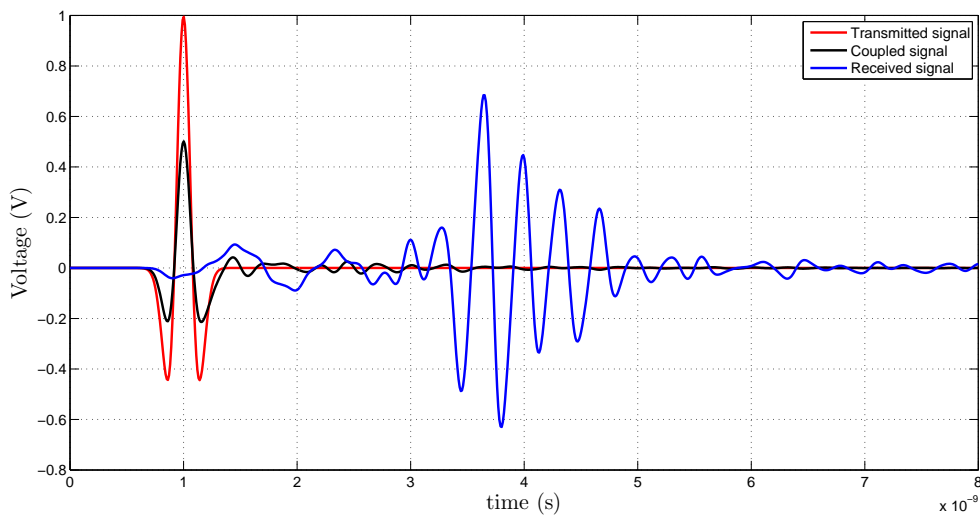


Figure 4.10: Implemented circuit in ADS



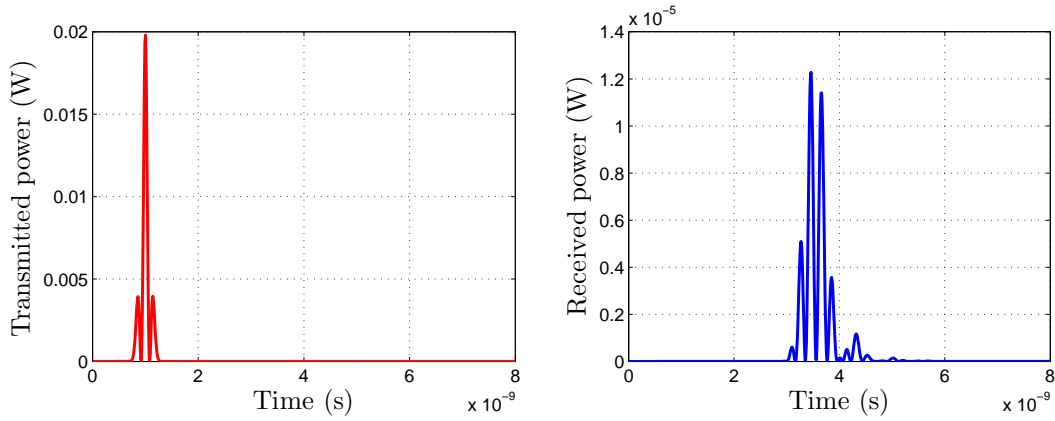
(a) Simulated antenna link



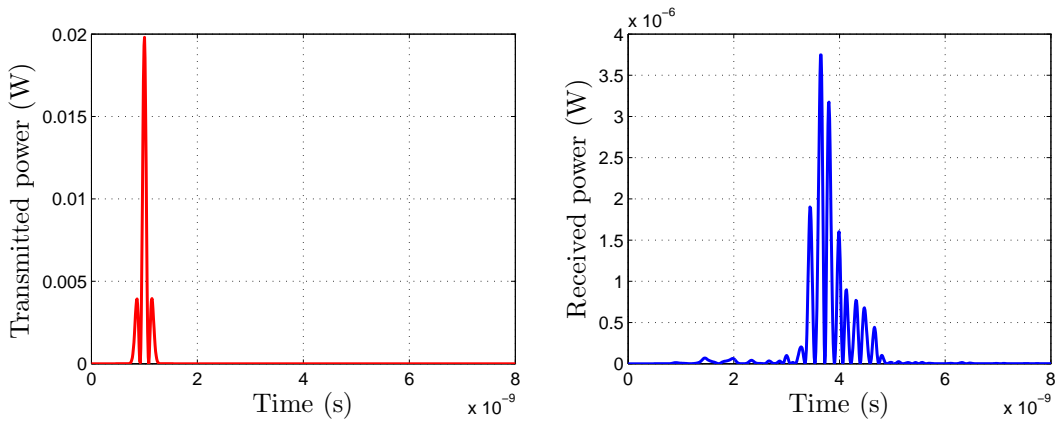
(b) Measured antenna link

Figure 4.11: Voltage Ricker wavelets at different circuit stages.

power graphs from the transmitted and received signals are shown in Fig. 4.12. Due to the signal has a resonant region probably caused by reflections from the ground and inside the antenna structure, we need to quantify the real pulse width from Fig. 4.12. For this, it was considered a signal amplitude greater than 10% of its maximum amplitude. Lower values were disregarded and the pulse width was calculated by simple subtraction. Table 4.2 contains the total pulse duration at output  $t_{p_{spread}}$  when the system was excited with the Ricker wavelet.



(a) Simulated antenna link



(b) Measured antenna link

Figure 4.12: Power pulses in the time-domain

Table 4.2: Signals pulse width.

Signal	Pulse width ( $t_{p_{spread}}$ )
Transmitted	0.69ns
Received (simulation)	0.8ns
Received (measurement)	1.39ns

As demonstrated in Table 4.2, the pulse width obtained from measurements was

1.39 ns. Therefore, the condition where the pulse width with dispersion  $t_{pspread}$  must be less or equal to  $t_{pmax}$  (defined as 3.46 ns in section 2.2) was satisfied.

After this analysis, it is possible to conclude that, although the antenna has some dispersive behavior, this behavior is low enough to allow separation of the reflections originated from pavement discontinuities.

## 4.5 Partial conclusions

Overall, this chapter presented a parametric optimization of the monopole antenna defined in chapter 3. The results allowed obtaining and validating a new optimum antenna adequate for the test pavement problem and impulse GPR applications.

Regarding the optimization process, it was observed that the solution of the multi-objective problem (impedance matching and gain) was not satisfactory. The algorithm converged favoring the gain over the impedance matching. A probable explanation of this can be that the antenna topology with the reflector plane has an ease to obtain high gain values, instead of wide impedance bandwidth. Then, it could be argued that the positive results of the algorithm were due to the simplification of the objective problem to optimize only the impedance bandwidth. However, the exclusion of the gain could be inappropriate and lead to an antenna with poor gain characteristics, which is not desired. The search for adequate gains was hand-crafted and it did not represent an interesting approach to obtain optimum GPR antennas. Furthermore, the antenna dispersion, which is a significant parameter to design GPR antennas, was not considered during the optimization process. All the dispersion analysis was performed *a-posteriori*.

On the other hand, it can be stated that solving the optimization problem in the frequency-domain with only a few (5) frequency points undersamples the objective functions, which can lead to inaccurate results. Therefore, a method to solve the optimization problem using a time-domain electromagnetic solver could avoid this undersampling issue. In this regard, the next chapter will present and evaluate the results of the optimization of the new single-objective function using a time-domain electromagnetic solver. The multi-objective problem will be analyzed again in order to compare both problems.

## Chapter 5

# Optimization approach using a time-domain electromagnetic solver

The findings in Chapter 4 helped us to evidentiate (prove) that a frequency-domain optimization approach is computationally expensive (even taken a few frequency points) and that the multi-objective problem is actually of difficult convergence. Therefore, this chapter shows the optimization results of the single-objective function proposed in this thesis and defined in Eq. 3.3. In addition, the optimization of the multi-objective problem was performed again given the change of the electromagnetic solver (HFSS to FDTD). This will allow us to establish a comparison of both problems and evaluate the effectiveness of the single-objective proposal.

A Finite-difference time-domain (FDTD) program was performed to calculate the objective functions. The program was adapted from [Elsherbeni and Demir, 2016] and implemented in MATLAB. This FDTD program was chosen because it is open-source and because it would be easy to adapt to the optimization algorithm.

Two antenna geometries, the monopole (Fig. 3.3) and the Vivaldi (Fig. 3.4), were implemented and simulated in FDTD. The FDTD algorithm divides the problem geometry into a spatial grid where electric and magnetic field components are placed at certain discrete positions in space, and it solves Maxwell's equations in time at discrete time instances [Elsherbeni and Demir, 2016]. This implies that the simulation time is dependent on the time steps and on the size of the grid elements.

Therefore, based on sensibility simulations, the size of the grid elements for the monopole antenna was settled to  $\Delta x = 1mm$ ,  $\Delta y = 1mm$ ,  $\Delta z = 0.8mm$  and for the Vivaldi antenna to  $\Delta x = 0.5mm$ ,  $\Delta y = 0.5mm$ ,  $\Delta z = 0.5mm$ . Each monopole antenna geometry was run with different time steps while the Vivaldi geometries maintained a fixed value of 5000. In this way, some computational time was saved without losing

information.

On the other hand, the optimization algorithms used in this chapter were parallelized to accelerate the optimization process. Thus, twelve cores allowed simulating twelve antenna geometries at the same time. For evaluating the reproducibility (confidence) of the obtained results, the number of optimization algorithms' executions is generally assumed from 10 to 100 [Carling and Meng, 2016]. However, such a high execution number would be impractical to our problem given the computational cost of each solution. Therefore, three executions of both the single- and multi-objective problems were performed for the monopole antenna in Fig. 3.3 and only one execution of each problem was performed for the Vivaldi antenna in Fig. 3.4.

In this chapter, the single-objective problem was solved using the parallel DE algorithm with population size  $N_{pop} = 24$  and number of generations  $gen = 30$ . The setting of DE operators was 0.3 and 0.5 for crossover and mutation, respectively. On the other hand, the multi-objective problem was solved using the parallel NSGA-II with population size  $N_{pop} = 24$  and number of generations  $gen = 30$ . The setting of NSGA-II operators was 1.2 and 0.1 for crossover and mutation, respectively. Both algorithms have the number of generations as the only stop criterion.

It is important to mention here that the initial simulations of the optimization problem in FDTD showed that a numerical error was being induced to the calculations of the directivity and, consequently in the gain. Following the notation of [Elsherbeni and Demir, 2016], the directivity is calculated as follows

$$\begin{aligned} D_{\theta} &= \frac{k^2}{8\pi\eta_0 P_{rad}} |L_{\phi} + \eta_0 N_{\theta}|^2 \\ D_{\phi} &= \frac{k^2}{8\pi\eta_0 P_{rad}} |L_{\theta} + \eta_0 N_{\phi}|^2 \end{aligned} \quad (5.1)$$

where  $k$  is the wave number expressed as  $k = 2\pi f \sqrt{\mu_0 \epsilon_0}$ ,  $\eta_0$  is the intrinsic impedance of free space,  $L_{theta}$  and  $N_{phi}$  are the auxiliary fields of the vector potentials approach [Elsherbeni and Demir, 2016] and  $P_{rad}$  is the radiation power defined as

$$P_{rad} = \frac{1}{2} Re \left\{ \int_S \vec{J}^* \times \vec{M} \cdot \hat{n} dS' \right\} \quad (5.2)$$

where  $\vec{J}$  and  $\vec{M}$  represent the equivalent surface electric and magnetic currents, respectively.

The numerical error emerged when the antenna had very low values (close to zero) of the s11 parameter. This means that the incoming energy to the antenna is

almost zero. Then, following the Eq. (5.2), the radiation power also tends to zero given the extremely low values of the equivalence surface currents. In the end, as Eq. (5.1) implies a division by  $P_{rad}$  (which is a near-to-zero value), the obtained directivity values were very high (in the order of 50 dB), as also the gain. This error allowed the optimization algorithm to generate viable mathematical solutions to the problem (antennas with apparently very high gain) but resulted in unworkable antennas.

As it was observed that this error was inherent to the implemented FDTD, the equation of realized gain was modified as shown in Eq. 5.3.

$$G_{mod} = e_{ff} \cdot D \cdot (1 - |s_{11}|^2) \quad (5.3)$$

where  $e_{ff}$  is the antenna efficiency,  $D$  is the directivity and  $s_{11}$  is the return loss.

As a consequence, a restriction to the algorithm is added using Eq. (5.3), making the gain value dependent on the  $s_{11}$  parameter and thus avoiding the numerical error. This process can be compared with the empirical attribution of objective function weights used by some authors to provide a balance between optimization time and accuracy or to seek the balance between the degree of wide impedance bandwidth and the degree of good impedance matching [Dumoulin et al., 2012, Chen and Chiu, 2016].

The time-domain analysis of the pulse in this chapter was performed in two ways: the first was the same defined in section 4.4 where the pulse width is calculated by simple subtraction disregarding values of power lower than 10% of its maximum amplitude. The second way is to evaluate the time shape of the radiated pulse in the angular direction of interest through the calculation of the fidelity factor (FF) as expressed in Eq. (5.4) [Quintero et al., 2011]. The  $\hat{S}_T(t)$  and  $\hat{S}_R(t)$  in Eq. (5.4) represent the normalized transmitting and received signals between two antennas, respectively. It is desirable that the antennas present fidelity factors greater than 0.5, otherwise the received signal would be unrecognizable [Quintero et al., 2011].

$$FF = \max_n \int_{-\infty}^{\infty} \hat{S}_T(t) \hat{S}_R(t + \tau) dt \quad (5.4)$$

where

$$\hat{S}_R(t) = \frac{S_R(t)}{\sqrt{\int_{-\infty}^{\infty} |S_R(t)|^2 dt}} \quad \hat{S}_T(t) = \frac{S_T(t)}{\sqrt{\int_{-\infty}^{\infty} |S_T(t)|^2 dt}}$$

## 5.1 Microstrip monopole antenna

### 5.1.1 Single-objective problem

Fig. 5.1 shows the convergence of the three executions. The red circles and the blue "xs" in Fig. 5.1 represent the best-found value and the mean of the objective function for each iteration, respectively. Also, it is shown on the top of each plot, the best cost function and mean, obtained at the last iteration. What can be clearly seen in Fig. 5.1 is that the algorithm did not converge prematurely to a solution and that the population was maintained diverse because the mean is distant from the best cost value on each iteration.

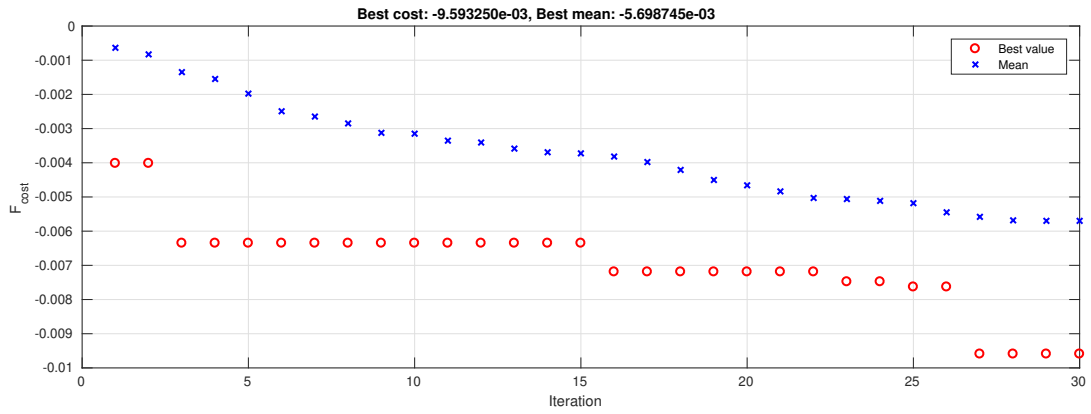
Besides this, it can be observed in Fig. 5.1 that each optimization algorithm execution led to similar results in terms of the cost function but not necessarily in terms of individuals (antenna geometry parameters). Therefore, the antenna parameters' diversity inside the search space was also plotted for the three algorithm executions to observe the behavior of the variables at the last iteration (See Fig. 5.2).

Figure 5.2 on the left side reveals that most parameter values are well-distributed, which means that the diversity on the search space was maintained. In turn, Fig. 5.2 on the right side shows the optimum antenna geometries obtained from each algorithm execution. As can be observed, the geometries are not equal between the three executions despite leading to an approximated objective function value.

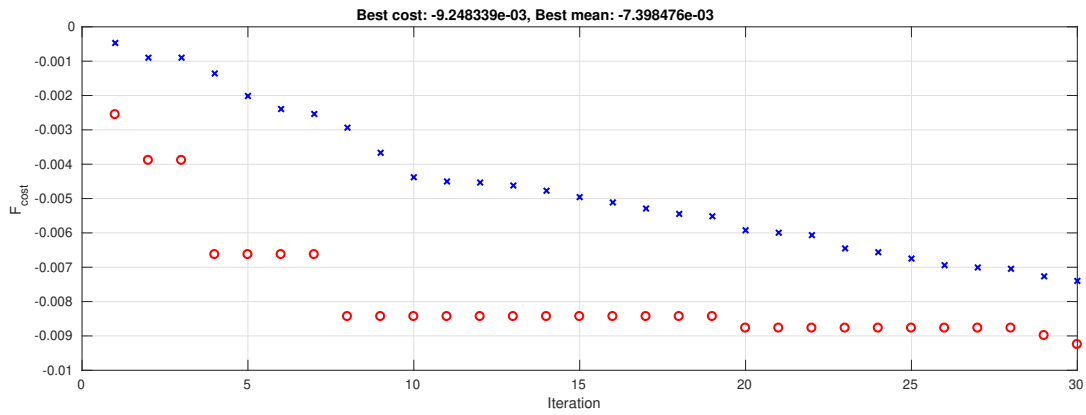
Table 5.1 presents the optimum antenna geometry parameters obtained on each execution. These antenna geometries were simulated separately where all the elements, microstrip line, patch, arms, ground, and reflector plane were modeled as perfect electric conductors (PECs), and a port was connected to the microstrip line as the feed. The PEC elements were all placed in an FR4 low-cost substrate considering  $\epsilon_r = 4.4$ , and  $\sigma = 0$ . The obtained results in the time- and frequency-domain are presented next.

Table 5.2 compares the total pulse duration  $t_{p_{spread}}$  and the fidelity factor of the antennas obtained from the three executions. It can be seen from the data in Table 5.2 that the three obtained antennas are good candidates for use in the GPR problem because a  $t_{p_{spread}}$  value that does not exceed  $t_{p_{max}}$  (defined as 3.46 ns in section 2.2) is desirable. Also, the antennas presented good fidelity factor values which means that the time shape of the received signal resembles the input signal. The antennas from execution 1 and 3 have almost the same pulse spread value but the last one presents the highest fidelity factor.

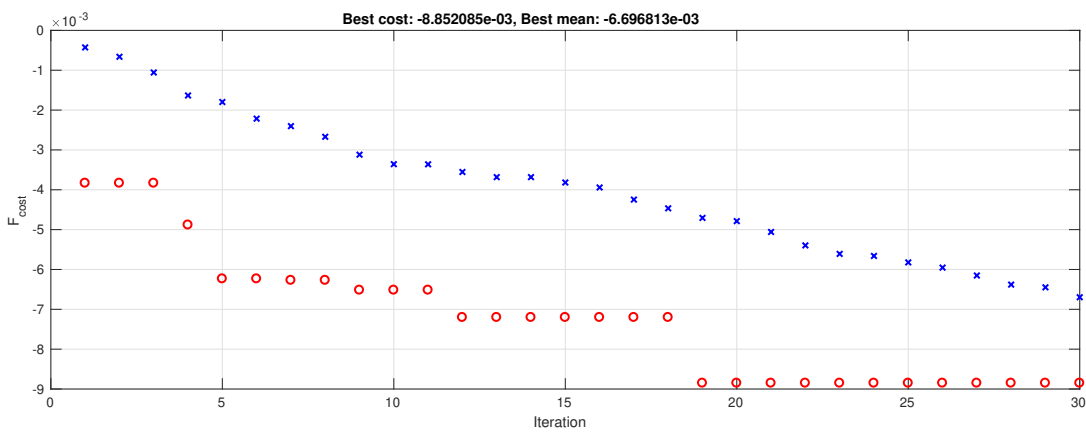
Fig. 5.3 shows the behavior of the  $s_{11}$  parameter and the gain in the desired frequency band to visualize how these two characteristics are correlated to generate



(a) First execution



(b) Second execution



(c) Third execution

Figure 5.1: Convergence of the single-objective problem for the monopole antenna.



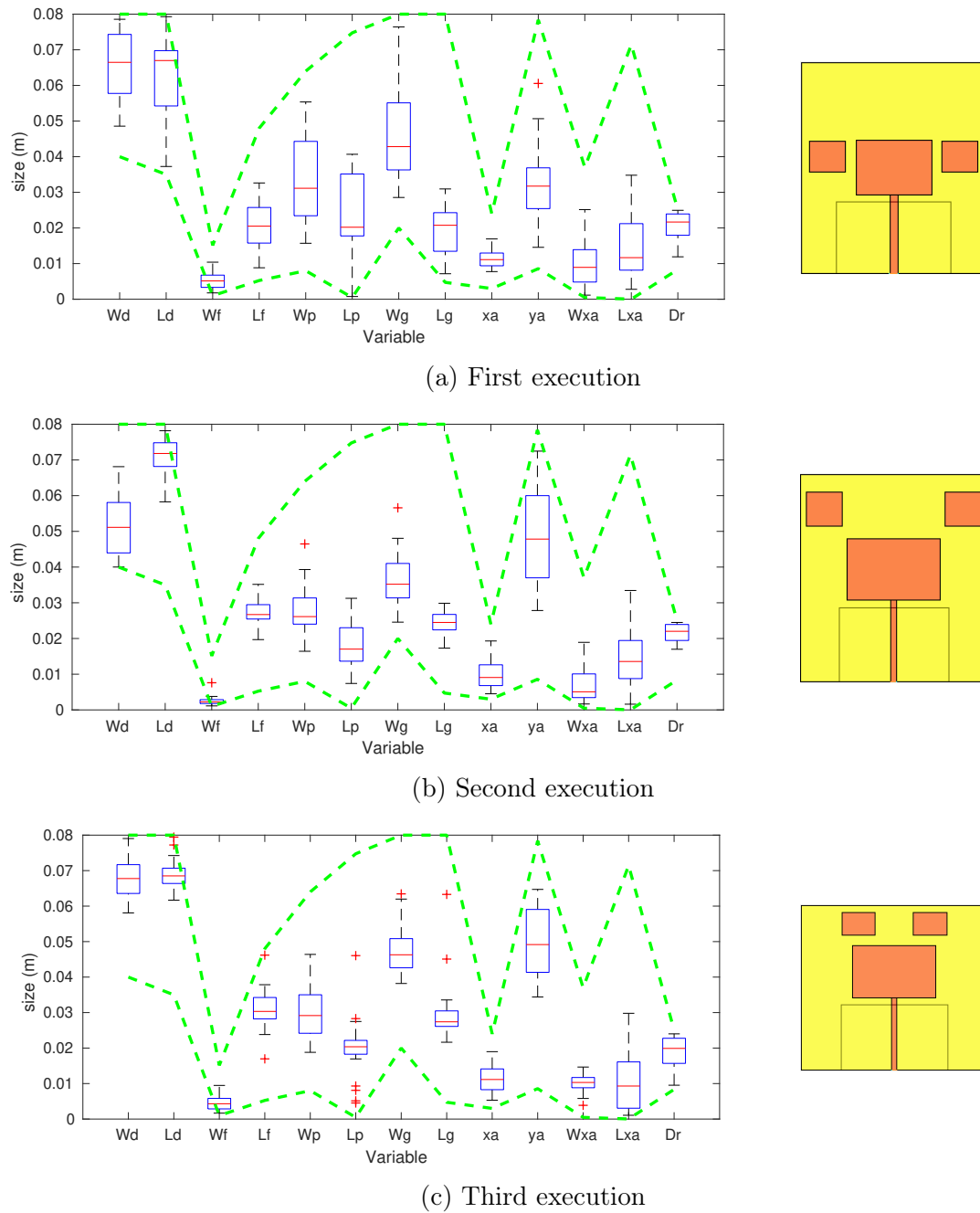


Figure 5.2: Boxplot of the monopole antenna variables (left) and best geometry (right) from the last generation.

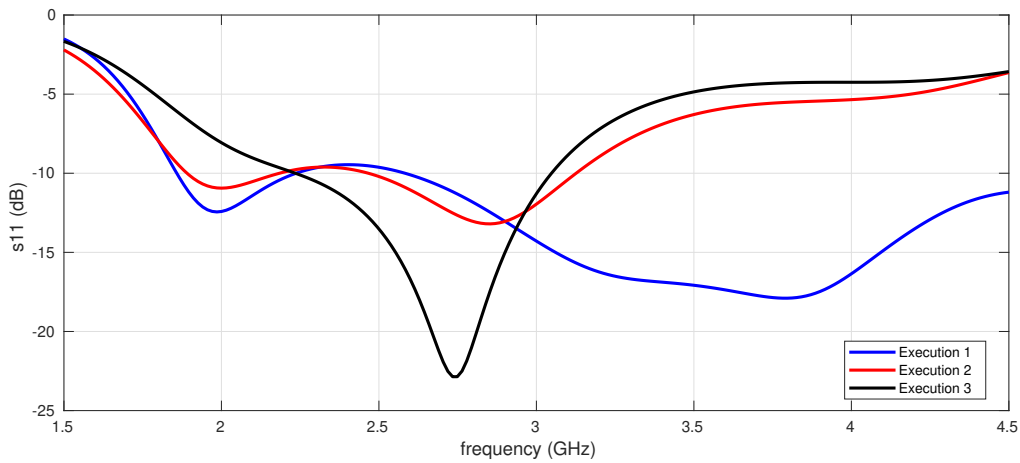
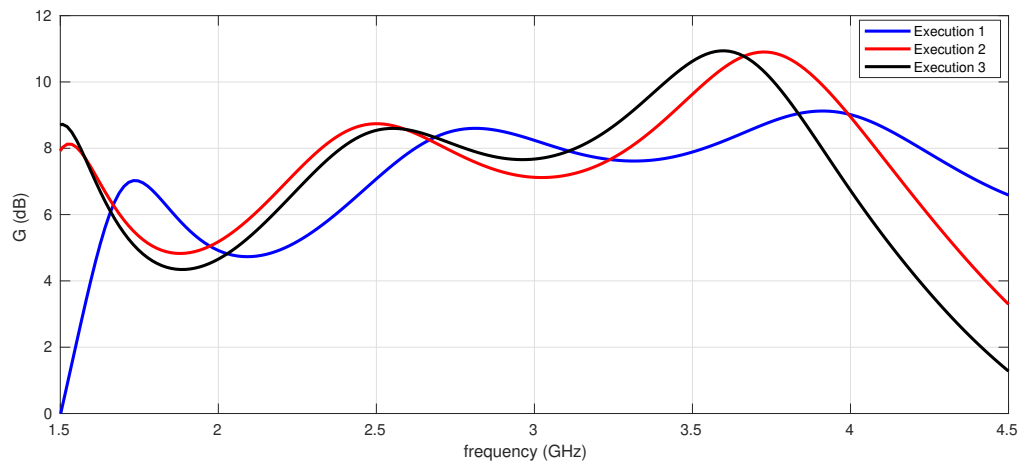
Table 5.1: New monopole antenna parameters obtained from the optimization of the single-objective problem

Parameter	Execution 1 Value (mm)	Execution 2 Value (mm)	Execution 3 Value (mm)
$W_d$	57	61	77
$L_d$	75	78	69
$W_f$	3	2	2
$L_f$	28	31	30
$W_p$	23	30	35
$L_p$	19	23	22
$W_g$	35	36	45
$L_g$	25	28	27
$x_a$	15	17	8
$y_a$	36	59	56
$W_{xa}$	11	12	14
$L_{ya}$	11	10	13
$dist$	24	22	19

Table 5.2: Time-domain results for monopole antenna from the single-objective problem optimization.

Execution	Pulse width ( $t_{p_{spread}}$ )	Fidelity factor (FF)
1	0.74 ns	0.884
2	0.82 ns	0.881
3	0.76 ns	0.896

antennas with good time-domain performance. From figure 5.3(a), we can see that the antenna from execution 1 reported significantly better  $s_{11}$  than the other two. Besides, it is shown in Fig. 5.3(b) that the gain for the three antennas has good similar responses having values ranging from 4.3 dB to 10.9 dB in almost all desired frequency components. Based on this result, it can be stated that the inclusion of the ground plane actually leads to improve the gain response of the monopole antenna, which traditionally extends up to 5 dB. The oscillations in the gain curve may occur because the reflector plane distance is defined around  $\lambda/4$  at the central frequency. This would suggest that at some frequencies the gain response would present lower values because the reflected signals are not in phase with the radiated ones.

(a)  $|s_{11}|$  in dB

(b) Realized gain in dB

Figure 5.3: Frequency-domain results for monopole antenna from the single-objective problem optimization.

### 5.1.2 Multi-objective problem

Turning now to the multi-objective problem, the optimization consisted of the minimization of the maximum  $s_{11}$  value and the maximum negative gain found in the frequency band of interest (1.5GHz - 4.5 GHz). This last function was modified from the original problem proposed in Eq. 3.1 where the gain was optimized only at the central frequency.

The results of this problem along with the respective diversity of the variables for the three algorithm executions are shown in Fig. 5.4. The left side of Fig. 5.4 shows the Pareto front with the non-dominated solutions (blue circles) and one of the best individuals obtained from the single-objective problem solution (red point).

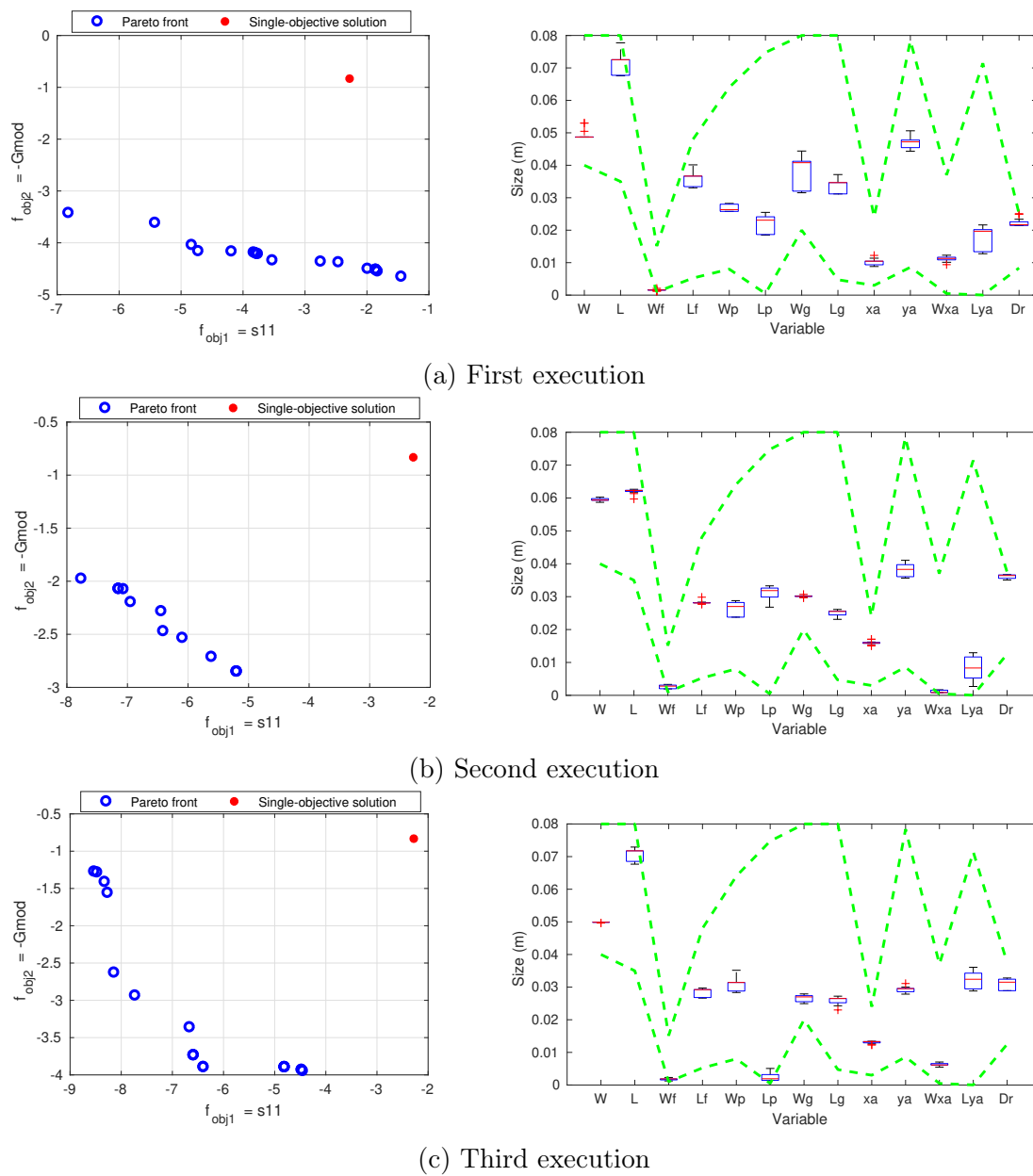


Figure 5.4: Pareto fronts of the multi-objective problem (left) and boxplot of the monopole antenna variables (right).

As can be seen in Fig. 5.4, the single-objective result is dominated by the Pareto solutions in the three executions. A probable explanation of this result is that the single-objective proposal intends to find an adequate correlation between the antenna characteristics and this does not necessarily imply only a good behavior of the gain and the s11 in the whole bandwidth but also in the phase response. Besides this, it is possible to observe in Fig. 5.4 the algorithm tendency to find extreme solutions that minimize one objective more than the other. Finally, the right side of Fig. 5.4 shows the

boxplots corresponding to the parameters diversity between the Pareto front solutions for each execution. It can be stated that the three executions of the multi-objective problem led to different antenna geometries.

All the antenna geometries from the Pareto fronts were simulated individually considering a FR-4 low cost substrate with  $\epsilon_r = 4.4$ , and  $\sigma = 0$ . The time-domain results are presented in Table 5.3. As can be seen from the table, all geometries meet the requirement of having a pulse width value ( $t_{p_{spread}}$ ) less than  $t_{p_{max}}$  defined as 3.46 ns. This means that all the antennas are candidate solutions for the test problem defined in section 2.2. However, some of them have slightly better values than the others.

Table 5.3: Time-domain results for monopole antenna from the multi-objective problem optimization.

Geometry	Execution 1		Execution 2		Execution 3	
	$t_{p_{spread}}$	FF	$t_{p_{spread}}$	FF	$t_{p_{spread}}$	FF
1	1.12 ns	0.794	1.14 ns	0.824	0.88 ns	0.866
2	1.19 ns	0.814	0.88 ns	0.828	0.88 ns	0.866
3	1.19 ns	0.813	0.88 ns	0.828	0.87 ns	0.849
4	1.18 ns	0.814	0.88 ns	0.828	0.86 ns	0.839
5	1.19 ns	0.815	0.88 ns	0.829	0.86 ns	0.866
6	0.91 ns	0.838	1.16 ns	0.819	0.91 ns	0.837
7	1.18 ns	0.814	1.14 ns	0.821	0.93 ns	0.828
8	0.91 ns	0.839	0.84 ns	0.875	0.92 ns	0.864
9	0.93 ns	0.838	0.84 ns	0.875	0.92 ns	0.861
10	0.93 ns	0.852	0.84 ns	0.875	0.95 ns	0.863
11	0.93 ns	0.845	0.79 ns	0.876	0.92 ns	0.861
12	0.93 ns	0.845	0.84 ns	0.862	0.94 ns	0.856
13	0.94 ns	0.844	0.84 ns	0.859	0.96 ns	0.866
14	0.94 ns	0.846	-	-	0.92 ns	0.861
15	0.98 ns	0.862	-	-	0.88 ns	0.846
16	0.96 ns	0.906	-	-	0.88 ns	0.846
17	0.96 ns	0.877	-	-	-	-
18	0.94 ns	0.872	-	-	-	-
19	0.95 ns	0.876	-	-	-	-

The geometries with the best time-domain characteristics, lowest dispersion value, and the highest fidelity factor were highlighted in Table 5.3 and its corresponding dimensions are shown in Table 5.4. In turn, the peak values of the received pulse amplitude for the antennas in Table 5.4 are listed in Table 5.5.

It is possible to observe in Table 5.5 that the peak values are very close to each other. A way to quantify this proximity is to calculate the coefficient of variation (CV) using Eq. (5.5).

Table 5.4: New monopole antenna parameters obtained from the optimization of the multi-objective problem

Parameter	Execution 1 Value (mm)	Execution 2 Value (mm)	Execution 3 Value (mm)
$W_d$	49	49	49
$L_d$	68	73	68
$W_f$	2	2	2
$L_f$	34	37	33
$W_p$	26	28	26
$L_p$	20	24	19
$W_g$	41	41	32
$L_g$	32	35	31
$x_a$	10	11	10
$y_a$	46	47	45
$W_{xa}$	10	11	11
$L_{ya}$	17	20	13
$dist$	23	22	23

$$CV = \frac{sd}{\bar{V}_p} \times 100\% \quad (5.5)$$

where  $sd$  is the standard deviation of the data and  $\bar{V}_p$  represents the mean of the peak values.

Table 5.6 shows the mean of the antenna peak values presented in Table 5.5 and its coefficients of variation. As can be seen, the peak values variation obtained for the antennas in the Pareto fronts of the three executions is low, which means that the dataset is homogeneous. The mean of the peak values can be compared with the peak values obtained in the single-objective problem solutions (Execution 1 - 9.58 mV, Execution 2 - 9.25 mV, Execution 3 - 8.85 mV). From this comparison, it can be stated that the obtained solutions in the multi-objective problem are near to the solutions of the single-objective problem, although, the latter presents higher values.

The frequency-domain results of the three highlighted antenna geometries in Table 5.3 were plotted and presented in Fig. 5.5. The simulated impedance matching is depicted in Fig. 5.5(a) and the antenna gain in fig. 5.5(b). It is possible to observe that geometries 11 (geo11) and 5 (geo5) present very similar responses in both frequency characteristics. The  $s_{11}$  parameter in geo 11 covered 75% of the desired bandwidth and in geo 5 63.3%. As well, the gain of the geo 11 presented values 1dB greater than geo 5 at frequencies higher than 2.7 GHz. On the other hand, geometry 8 showed a narrow bandwidth and the highest peak gain: 9 dB. These results in the impedance

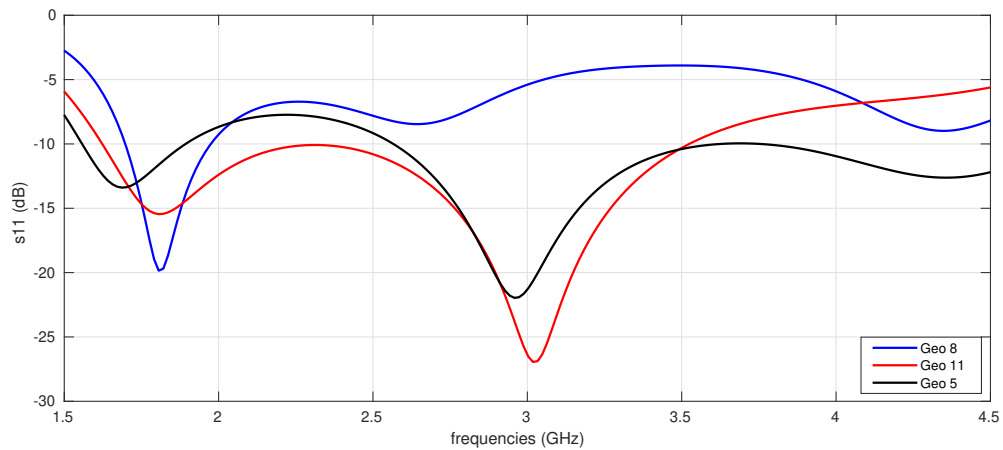
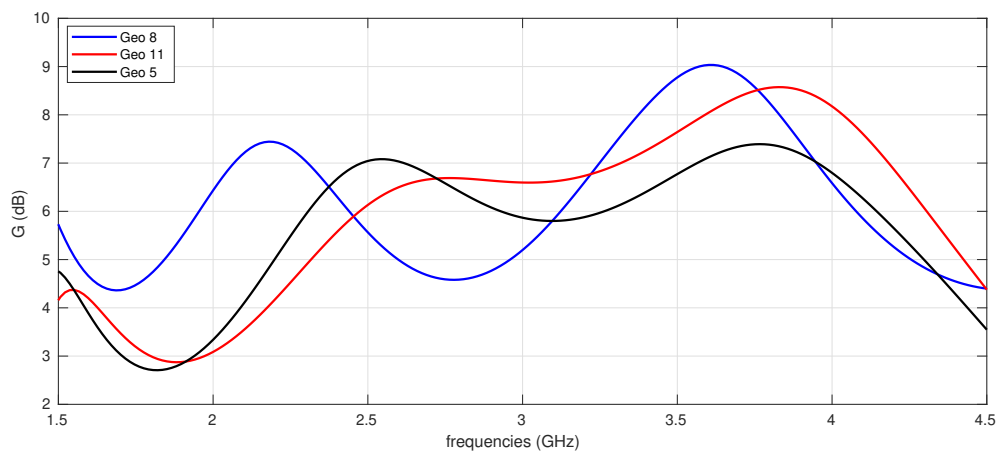
Table 5.5: Peak values of the received pulse for the best antennas of the multi-objective problem.

	<b>Execution 1</b>	<b>Execution 2</b>	<b>Execution 3</b>
<b>Geometry</b>	<b>Peak value (mV)</b>	<b>Peak value (mV)</b>	<b>Peak value (mV)</b>
1	7.259	6.066	8.467
2	7.333	5.786	8.467
3	7.281	5.786	6.708
4	7.267	5.786	6.429
5	7.268	5.785	7.605
6	7.886	6.161	6.736
7	7.267	6.165	6.714
8	7.494	7.356	8.918
9	7.525	7.355	8.886
10	7.983	7.356	8.632
11	7.825	7.835	8.886
12	7.825	6.665	8.599
13	7.730	6.635	8.902
14	7.770		8.886
15	8.089		7.569
16	9.126		7.569
17	8.117		
18	8.498		
19	8.495		

Table 5.6: Coefficient of variation of the data on Table 5.5

	<b>Execution 1</b>	<b>Execution 2</b>	<b>Execution 3</b>
$V_p$	7.79 mV	6.52 mV	8 mV %
CV	3.33 %	2.84 %	1.43 %

matching can be a consequence of the definition of the multi-objective problem where the algorithm tends to find extreme solutions that minimize one objective more than the other. On the other hand, the gain curves in Fig 5.5(b) presented values ranging from 3 to 9 dB. This means that the inclusion of the reflector plane allowed obtaining better gain values in the desired frequency band, as it was also shown and explained for the gain curves on the single-objective solutions.

(a)  $|s_{11}|$  in dB

(b) Realized gain in dB

Figure 5.5: Frequency-domain results for monopole antenna from the multi-objective problem optimization.

## 5.2 Exponentially tapered slot antenna - Vivaldi

### 5.2.1 Single-objective problem

Fig. 5.6 presents the convergence of the optimization problem. The best-found solutions and the population mean of each generation are represented by the red circles and the blue "xs", respectively. Also, the top of Fig. 5.6 shows the best value of the objective function and its mean.

It can be stated from Fig. 5.6 that the algorithm did not converge prematurely to a solution. However, the population has likely dropped its diversity given that the mean is close to the best value. To observe this, Fig. 5.7 shows the boxplot of the variables' diversity in the search space at the last iteration and the best antenna



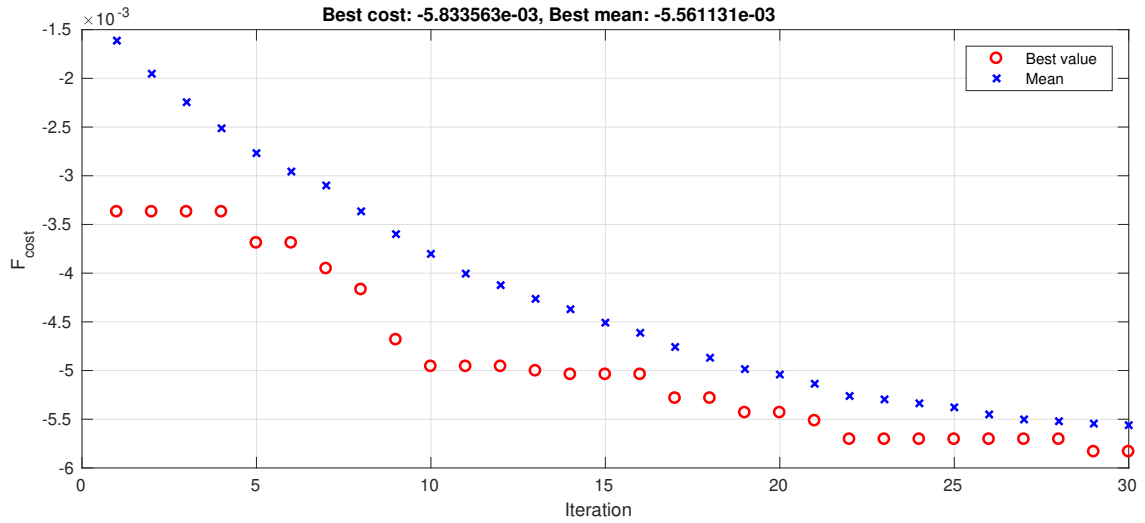


Figure 5.6: Convergence of the single-objective problem for the Vivaldi antenna.

geometry obtained from the optimization process. The variable *Rate* in Fig. 5.7 was normalized from 0 to 1 to appear on the plot because its values are dimensionless and high. In Fig. 5.7 there is a clear trend of diversity decreasing, especially in the variables *s*, *La*, *Wm*, and *Qwm*. However, these values were very restricted from the beginning to limit the search space and were based on recommendations in the literature.

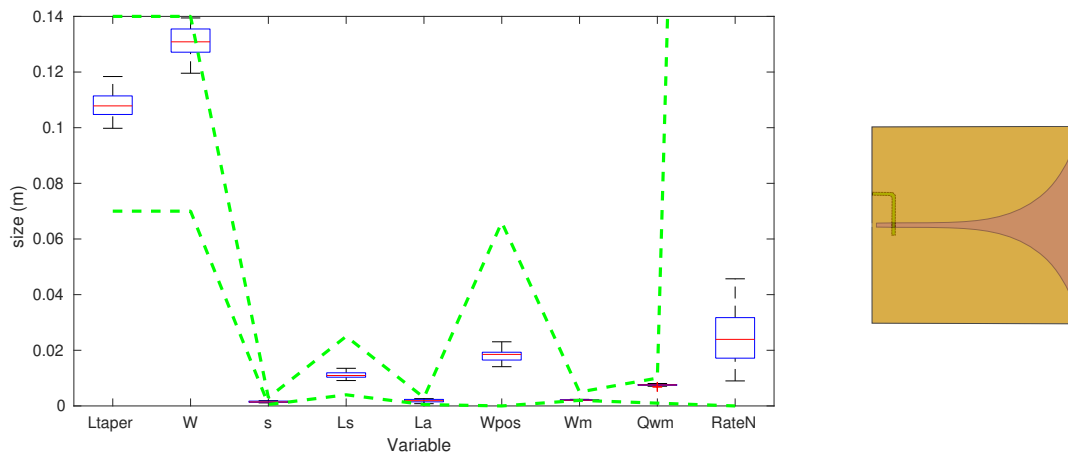


Figure 5.7: Boxplot of the Vivaldi antenna variables (left) and best geometry (right) from the last generation.

Table 5.1 presents the optimum antenna geometry parameters. This antenna was simulated separately and the results in time- and frequency-domain are presented next.

The total pulse duration  $t_{p_{\text{spread}}}$  and the fidelity factor of the antenna are listed in Table 5.8. As can be seen from the table, the time-domain results indicate that the

Table 5.7: New Vivaldi antenna parameters obtained from the optimization of the single-objective problem

Parameter	Value
$L_{taper}$	111.5 mm
$W_d$	127.5 mm
$s$	1.5 mm
$L_s$	11 mm
$L_a$	2.5 mm
$W_{pos}$	18.5 mm
$W_m$	2 mm
$Q_{wm}$	8 mm
$Rate$	51.35
$RateN$	0.009

Table 5.8: Time-domain results for Vivaldi antenna from the single-objective problem optimization.

Pulse width ( $t_{p_{spread}}$ )	Fidelity factor (FF)
0.8 ns	0.9

obtained Vivaldi antenna is adequate for use in the specific application proposed in section 2.2. A pulse width of 0.8 ns meets the condition of a pulse width less than 3.46 ns. Besides, the designed antenna reaches a high fidelity factor which allows better detection of the received pulse.

The frequency antenna characteristics are presented in Fig. 5.8. From Fig. 5.8(a), it is possible to observe that the antenna has a bandwidth from 1.8 GHz to 4.1 GHz which covers almost all (76.6%) the desired frequency band. This agrees with the wide bandwidth characteristic of the Vivaldi antenna. The behavior of the impedance matching near to the frequency bounds could be explained by the fact that the Ricker wavelet concentrates most energy around the central frequency. Therefore, the energy on the frequency bounds may not contribute that much to the maximization of the received signal making the algorithm converge to this solution. However, further investigations should be performed to corroborate it.

In turn, Fig. 5.8(b) presents the realized gain where the value is ranging from 3 dB to 6.5 dB at frequencies higher than 1.6 GHz. This gain response was expected since the maximum bound constraint of the exponentially tapered slot length was proposed smaller than one wavelength at the lowest frequency, instead of greater as suggested in [Balanis, 2016, p. 498]. Despite this, the antenna presented admissible gain values.

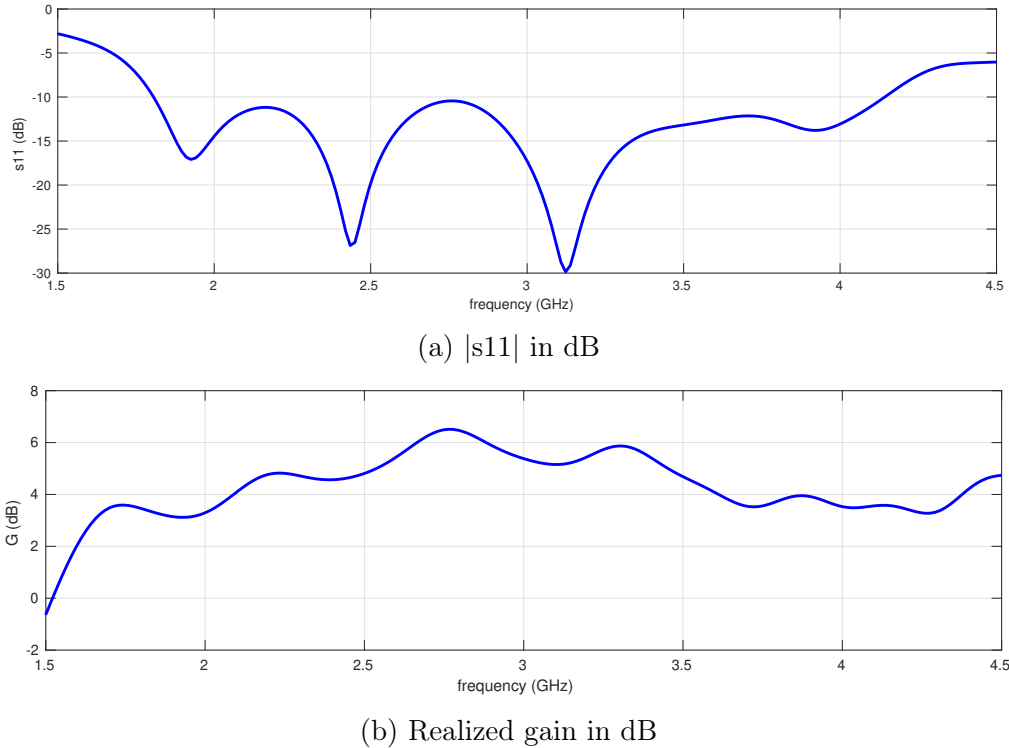


Figure 5.8: Frequency-domain results for Vivaldi antenna from the single-objective problem optimization.

## 5.2.2 Multi-objective problem

Moving on now to consider the multi-objective problem, the objective functions are the same ones evaluated in section 5.1.2 for the monopole antenna: the maximum  $s_{11}$  parameter and the lower gain in the frequency band of interest (1.5 GHz- 4.5 GHz).

The solution of this problem is shown on the left side of Fig. 5.9 where the blue circles are the non-dominated solutions of the multi-objective problem and the red point represents the worst frequency band values of  $s_{11}$  and gain of the single-objective problem solution obtained in section 5.2.1. As can be observed on the left side of Fig. 5.9, the extrapolated solution from the single-objective problem is dominated by the solutions in the Pareto front. These results agree with the ones obtained for the monopole antenna given that, as explained before, the single-objective problem is a metric of quality that intends to find the best correlation of the antenna characteristics, including the phase response, on the bandwidth of interest and not only in one frequency point.

The right side of Fig. 5.9 shows the boxplots corresponding to the variables diversity of each solution in the Pareto front. It can be seen that the antenna parameters are very close to each other, although different substrate sizes, represented by  $L_{taper}$

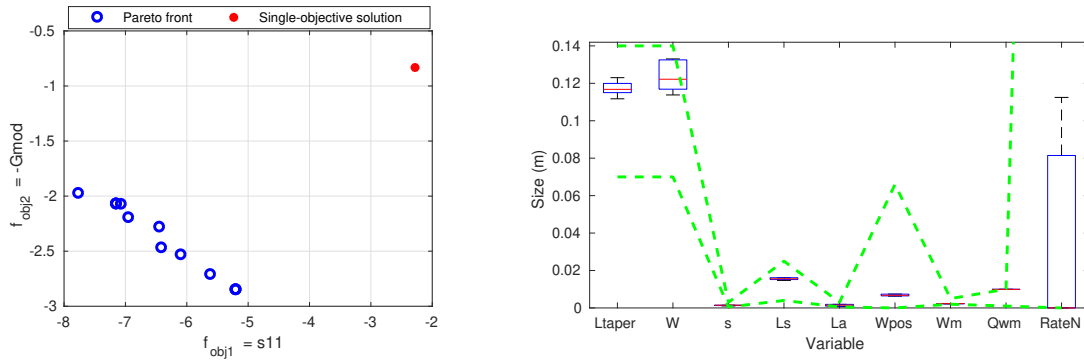


Figure 5.9: Pareto front of the multi-objective problem (left) and boxplot of the Vivaldi antenna variables (right).

and W, and exponential aperture (Rate) led to slightly different antennas.

All the eight antenna geometries presented in the Pareto front were simulated individually considering a FR-4 low cost substrate with  $\epsilon_r = 4.4$ , and  $\sigma = 11.7 \times 10^{-3}$ . The time-domain results are presented in Table 5.9. From the pulse width shown in Table 5.9, it is possible to affirm that all geometries meet the requirement of having a pulse width less than  $t_{pmax}$ , previously defined as 3.46 ns. Therefore, the obtained Vivaldi antennas are candidate solutions for the test problem defined in section 2.2.

Table 5.9 also shows the peak values of the received pulse amplitude obtained for each antenna. The coefficient of variation and the mean of this dataset were calculated using Eq. (5.5) and the results were:  $CV = 3.33\%$  and  $\bar{V}_p = 5.52$  mV. From these results, it can be stated that the dataset has low variability which means the data is homogeneous. Besides, comparing the mean of the antenna's peak values, the result of the multi-objective problem ( $\bar{V}_p = 5.52$  mV) is close but under to the single-objective problem solution which presented a peak value of 5.83 mV.

Table 5.9: Time-domain results for Vivaldi antenna from the multi-objective problem optimization.

Geometry	Pulse peak (mV)	$t_{pspread}$	FF
1	5.582	0.98 ns	0.862
2	5.629	0.82 ns	0.870
3	5.636	0.78 ns	0.867
4	6.003	0.82 ns	0.873
5	4.894	0.79 ns	0.883
6	5.682	1.03 ns	0.877
7	4.909	0.79 ns	0.889
8	5.827	0.82 ns	0.873

The solutions with the best time-domain pulse width and the best fidelity fac-

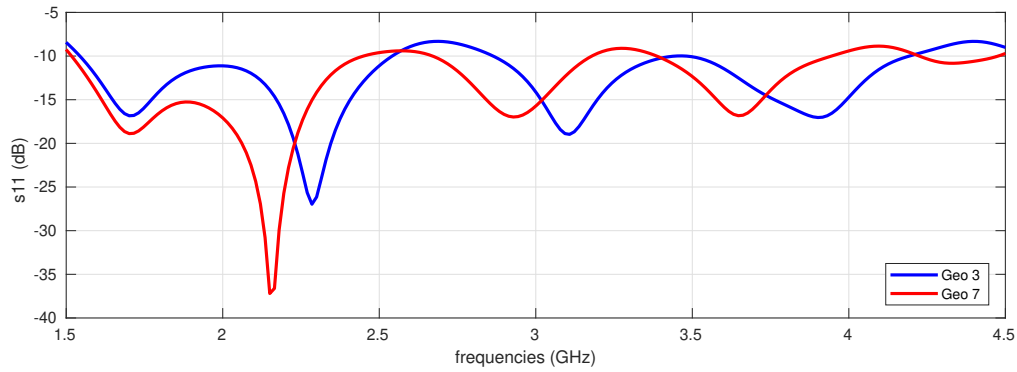
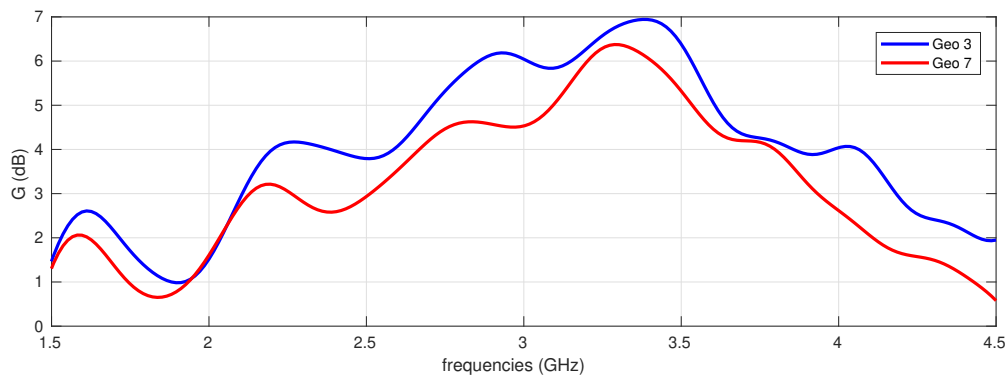
tor were highlighted in Table 5.9. The corresponding dimensions of the highlighted antennas (geometry 3 and geometry 7) are shown in Table 5.10.

Table 5.10: New Vivaldi antenna parameters obtained from the optimization of the multi-objective problem

<b>Parameter</b>	<b>Geometry 3 Value (mm)</b>	<b>Geometry 7 Value (mm)</b>
$L_{taper}$	115.5 mm	121.5 mm
$W_d$	120 mm	114 mm
$s$	1.5 mm	1.5 mm
$L_s$	16 mm	15 mm
$L_a$	2 mm	1 mm
$W_{pos}$	9 mm	10.5 mm
$W_m$	2.5 mm	2.5 mm
$Q_{wm}$	10 mm	10 mm
$Rate$	50	66.87
$RateN$	0	0.1125

The frequency-domain results of the two highlighted geometries were plotted and presented in Fig. 5.10. The simulated impedance matching is depicted in Fig. 5.10(a) and the antenna gain in Fig. 5.10(b). It is possible to observe that each geometry presents very similar responses in both frequency characteristics. Geometry 3 covered 78% of the desired impedance bandwidth and Geometry 7 a 75%. Again, the obtained Vivaldi antennas exhibited the wide bandwidth, characteristic of this topology.

On the other hand, Geometry 3 presented a higher gain than Geometry 7 in all the desired frequency band, ranging from 1 dB to 7 dB. As explained for the gain of the single-objective problem solution, the antenna gain responses in Fig. 5.10(b) exposed the same moderate gain values due to the limitation on the length of the exponentially tapered slot.

(a)  $|s_{11}|$  in dB

(b) Realized gain in dB

Figure 5.10: Frequency-domain results for Vivaldi antenna from the multi-objective problem optimization.

### 5.3 Partial conclusions

To sum up, this chapter presented the optimization results obtained using a time-domain electromagnetic solver. The new single-objective function results were compared with the traditional multi-objective ones for two different antenna topologies: the monopole and the Vivaldi. For all the evaluated optimization problems and antenna topologies, it was possible to obtain low-cost and compact solutions that met the time-domain requirement defined from the test pavement problem.

We are aware that our research used two different algorithms to evaluate the optimization problems and that this may have some influence on the results. However, as there was not a synchronization process of the algorithms operators, we believe that the results can be compared.

The results of the Vivaldi antenna optimization have revealed that the bounds constraints selected for the parameters were very restrictive. These values were limited to obtain compact antennas and a reasonable computational cost. Further studies,

which take these bounds into account, will need to be undertaken.

As presented, the multi-objective problem was solved using the time-domain electromagnetic solver (FDTD). The use of FDTD allowed performing a greater sampling of the objective functions at a reasonable cost. The multi-objective problem is still computationally expensive, taking one week to solve the monopole antenna geometry optimization and two weeks to solve the Vivaldi. However, solving the problem using FDTD represents a better approach since the undersampling issue is avoided.

In general, it is known that impedance matching is an important antenna characteristic because it allows minimize losses and adjusting the antenna bandwidth. This leads to desiring solutions with  $s_{11}$  parameter responses below -10 dB. However, as observed in the solutions of both problems, some  $s_{11}$  values are not below -10 dB in the whole bandwidth. This contradictory result could be attributed to the compensating effect between the goals. This means that perhaps the objectives ( $s_{11}$ , gain, phase) can be relaxed to obtain a low-distortion antenna.

Our findings from the single-objective proposal would seem to suggest that the  $s_{11}$  parameter region near the frequency bounds (1.5 GHz and 4.5 GHz) are not very significant to maximize the received signal. A probable cause of this can be the use of the Ricker wavelet, which presents low energy in those regions and could lead the algorithm to obtain those results. Despite that this tendency was observed, it cannot be considered a conclusion because there is not enough data to establish it yet.

Taken together, the results from the single-objective function suggest that the proposed metric represents an alternative to the traditional frequency-domain objective functions to develop optimum antennas. Besides, the single-objective function facilitates the antenna design process avoiding convergence problems and any decision-making process.

# Chapter 6

## Final Considerations

### 6.1 Conclusions

This thesis has highlighted the importance of an adequate detection of the reflected peaks measured by an impulse GPR to improve the solution technique of the multilayer inverse problem. For this purpose, the focus of this thesis was the optimum antenna design dedicated to homogeneous and low-loss dielectric multilayer media.

We have devised a new practical step-by-step methodology to obtain specific antenna requirements (its operating frequency and temporal response) through the analysis of the specific multilayer problem. In this way, the proposed methodology enables the production of specific antennas for the analyzed homogeneous and low-loss dielectric multilayer problem, serving as a practical guide for GPR antenna design

A pavement problem was defined as a case study to estimate the antenna requirements using the proposed methodology. Then, to fulfill the obtained requirements an optimization process was performed. As presented throughout the text, several authors addressed in the literature the UWB antenna optimization, although the proposals generally comprise contradictory multi-objective problems of difficult convergence. Besides, there is no consensus between the authors about the best way to align all the desired antenna characteristics (wide frequency bandwidth, good gain, and radiation efficiency, good impedance matching, and low dispersion). Therefore, we have explored two ways of defining the optimization problem. The first one was based on the traditional approaches where the impedance matching and the gain were optimized. The second one consisted of a new objective function proposal based on the maximization of the time-domain signal received by the antenna.

Chapter 4 comprised the evaluation of the traditional multi-objective problem (impedance matching and gain) of a monopole antenna with a reflector in the frequency-



domain. From the results, it was concluded that the problem is of difficult convergence and computationally expensive. Hence, as an alternative, the problem was simplified to optimize the more difficult objective to be fulfilled, the impedance matching. Finally, a new low-cost compact monopole antenna was obtained to satisfy the requirements. The antenna validation results using measurements showed low dispersive behavior, which indicates that there will be no overlap of the GPR reflected signals.

Even though an antenna for GPR impulse applications was obtained and validated, the optimization process was not very efficient. The gain was excluded from the optimization because the solutions of the multi-objective problem had tended to only improve the gain and not the impedance matching. This is not appropriate because it could lead to antennas with poor gain characteristics. Besides, it was stated that solving the objective function in the frequency-domain requires high computational cost. This was handled by taking only a few frequency points but lead to undersampling the function, which is not desired. On the other hand, the time-domain antenna dispersion, which is a significant parameter to design antennas for impulse GPR systems, was not addressed through the analyzed objective functions.

Chapter 5 presented the optimization results of the new single-objective function for two different antenna topologies: the monopole and the Vivaldi, using a time-domain electromagnetic solver. Our objective function proposal was based on the idea that the only way of increasing the amount of energy in the region of interest is through an adequate performance in all antenna characteristics. In this way, a single quality metric that aligns the common goals was defined for the GPR antenna design. The traditional multi-objective problem was also solved in Chapter 5 to compare both problems and to evaluate the effectiveness of the single-objective proposal.

The results of the single- and multi-objective problems using the time-domain solver (FDTD) allowed obtaining low-cost antennas with different topologies and reduced dispersion characteristics for impulse GPR applications. The solutions of the multi-objective optimization using FDTD were always non-dominated compared with the single-objective ones. Nevertheless, the Pareto solutions show the worst objective function values found but not the behavior of them in all the desired frequency band. For instance, an  $s_{11}$  parameter of -5 dB as the worst value can build both:  $s_{11}$  values around -5 dB in the whole bandwidth or  $s_{11}$  values ranging mostly down the -10 dB. Therefore, this can lead to a non-efficient solution in terms of bandwidth. Instead, our single objective function proposal will consider, at the same time, all the frequency components of the antenna characteristics (gain, impedance, and phase) to obtain an adequate received signal in the time-domain. Besides this, the optimization process using the new metric led directly to the optimum antenna without any later evaluation

or decision-making process. Therefore, the single-objective problem eases obtaining optimal solutions and the antenna design process.

Overall, it can be concluded from the findings in this thesis that the proposed methodology contributes to obtaining GPR equipment with higher precision in layer estimation. Besides, our single-objective proposal that aligns and weighs the common antenna characteristics represents a significant and easier approach (alternative path) to obtain optimum low-cost impulse GPR antennas with low dispersion. Additionally, this single metric can benefit all directive UWB antenna designs, not just those for GPR.

## 6.2 List of publications

The following publications have been performed during the development of this thesis:

- Africano, M., Vargas, J., Adriano, R., Oliveira, D., and Lisboa, A. (2020). Ground - penetrating radar antenna design for homogeneous and low-loss dielectric multilayer media. *Journal of Microwaves, Optoelectronics and Electromagnetic Applications*, 19(2):137 - 151.
- Artur, N., Contreras, M. V., Adriano, R., Resende, U. d. C., and Mologni, J. F. (2017). Uncertainties minimization in open environment antenna gain estimations. In *2017 IEEE 3rd Global Electromagnetic Compatibility Conference (GEMCCON)*, pages 1 - 5. IEEE.
- Pimenta, R., Africano, M., Adriano, R., and Resende, U. (2017). 3D CUDA FDTD based method for analysis of microstrip antennas. In *2017 SBMO/IEEE MTT-S International Microwave and Optoelectronics Conference (IMOC)*, pages 1 - 5. IEEE.

## 6.3 Continuity proposal

The development of this thesis needed to be delimited into some important aspects that can be explored in detail in further studies. In this way, the continuity proposals are related mainly to the following ideas:

- **Calculating the received signal directly from the time-domain.** In this thesis, the change from a frequency-domain solver to a time-domain solver was performed intending to account for the antenna dispersive characteristic directly

through the time-domain signal. In this way, the obtention of the objectives would be faster than the ones obtained in the frequency-domain solver. However, the process to compute the received signal was calculated from the frequency-domain antenna characteristics. Therefore, implementing Green's functions in the time-domain to estimate the received signal would improve the optimization process.

- **Considering the derivative antenna characteristic.** Several authors have stated that the antenna has derivative characteristics [Kanda, 1983, Sheng et al., 2003, Chamaani et al., 2011]. Therefore, a greater focus on the transmission of a Gaussian pulse or its first derivative could produce interesting findings that possibilities the output of a Ricker wavelet with the desired characteristics.
- **Selecting different input GPR signal.** The inquiring GPR signal selected for the optimum GPR antenna design was the Ricker wavelet because of its properties and widely use in the literature. However, the response of the optimization problems to variations on the input pulses types can be studied. This would allow knowing the sensibility of the problems to those variations and if the tendency of the antenna characteristics changes.
- **Syntonizing optimization algorithms.** Given that part of the focus in this thesis was on the proposal of an adequate optimization problem to find optimum antennas, there is a possibility that better results would have arisen if, besides the proposal, the improvement of the optimization algorithms was considered. This means selecting adequate and syntonized algorithm operators or even approximation models, like the one proposed in [Valadão, 2020], to decrease the high computational cost of the problem.
- **Vivaldi antenna exploration.** In this thesis, the Vivaldi antenna was analyzed and optimized. However, our initial concern was to obtain compact solutions for GPR applications at a reasonable computational cost. Consequently, the selected bound constraints were very restrictive. Therefore, we believe that the Vivaldi antenna results can be improved. Further studies can be related to the relaxation of the bound constraints or even to the use of different feeding geometries.

# References

- [Africano, 2015] Africano, M. (2015). A multimodal inverse problem for GPR pavement parameter estimation. Master's thesis, Universidade Federal de Minas Gerais, Brasil.
- [Africano et al., 2020] Africano, M., Vargas, J., Adriano, R., Oliveira, D., and Lisboa, A. (2020). Ground-penetrating radar antenna design for homogeneous and low-loss dielectric multilayer media. *Journal of Microwaves, Optoelectronics and Electromagnetic Applications*, 19(2):137–151.
- [Ahmed et al., 2016] Ahmed, A., Zhang, Y., Burns, D., Huston, D., and Xia, T. (2016). Design of UWB antenna for air-coupled impulse ground-penetrating radar. *IEEE Geoscience and Remote Sensing Letters*, 13(1):92–96.
- [Ali et al., 2017] Ali, J., Abdullah, N., Ismail, M. Y., Mohd, E., and Shah, S. M. (2017). Ultra-wideband antenna design for GPR applications: A review. *International Journal of Advanced Computer Science and Applications*, 8(7):392–400.
- [ANSI, 2013] ANSI (2013). American national standard of procedures for compliance testing of unlicensed wireless devices. *C63.10*, page 102.
- [Arezoomand et al., 2017] Arezoomand, A. S., Naser-Moghadasi, M., Arghand, I., Jahangiri, P., and Zarrabi, F. B. (2017). Photonic band gap implementation for phase centre controlling in vivaldi antenna. *IET Microwaves, Antennas & Propagation*, 11(13):1880–1886.
- [Artur et al., 2017] Artur, N., Contreras, M. V., Adriano, R., Resende, Ú. d. C., and Mologni, J. F. (2017). Uncertainties minimization in open environment antenna gain estimations. In *2017 IEEE 3rd Global Electromagnetic Compatibility Conference (GEMCCON)*, pages 1–5. IEEE.
- [Balanis, 2016] Balanis, C. A. (2016). *Antenna theory: analysis and design*. John Wiley & sons.

- [Beben et al., 2013] Beben, D., Anigacz, W., and Ukleja, J. (2013). Diagnosis of bedrock course and retaining wall using GPR. *NDT & E International*, 59:77–85.
- [Benedetto and Benedetto, 2002] Benedetto, A. and Benedetto, F. (2002). GPR experimental evaluation of subgrade soil characteristics for rehabilitation of roads. *Ninth International Conference on Ground Penetrating Radar*, 4758:708–714.
- [Benedetto and Pajewski, 2015] Benedetto, A. and Pajewski, L. (2015). *Civil engineering applications of ground penetrating radar*. Springer.
- [Benedetto and Pensa, 2007] Benedetto, A. and Pensa, S. (2007). Indirect diagnosis of pavement structural damages using surface GPR reflection techniques. *Journal of Applied geophysics*, 62(2):107–123.
- [Bhattacharjee et al., 2020] Bhattacharjee, A., Bhawal, A., Karmakar, A., Saha, A., and Bhattacharya, D. (2020). Vivaldi antennas: a historical review and current state of art. *International Journal of Microwave and Wireless Technologies*, pages 1–18.
- [Boylestad and Nashelsky, 2013] Boylestad, R. L. and Nashelsky, L. (2013). *Electronic devices and circuit theory*. Pearson.
- [Cai et al., 2016] Cai, J., Liu, S., Fu, L., and Feng, Y. (2016). Detection of railway subgrade moisture content by GPR. In *2016 16th International Conference on Ground Penetrating Radar (GPR)*, pages 1–5. IEEE.
- [Carling and Meng, 2016] Carling, K. and Meng, X. (2016). On statistical bounds of heuristic solutions to location problems. *Journal of combinatorial optimization*, 31(4):1518–1549.
- [Chamaani and Mirtaheri, 2010] Chamaani, S. and Mirtaheri, S. (2010). Planar uwb monopole antenna optimization to enhance time-domain characteristics using pso. *Aeu-international Journal of Electronics and Communications*, 64:351–359.
- [Chamaani et al., 2011] Chamaani, S., Mirtaheri, S. A., and Abrishamian, M. S. (2011). Improvement of time and frequency domain performance of antipodal vivaldi antenna using multi-objective particle swarm optimization. *IEEE Transactions on Antennas and Propagation*, 59(5):1738–1742.
- [Chen, 2016] Chen, Y. (2016). Frequency-domain and time-domain performance enhancements of ultra-wideband antennas using multiobjective optimization tech-

- niques. In *2016 10th European Conference on Antennas and Propagation (EuCAP)*, pages 1–4.
- [Chen and Chiu, 2016] Chen, Y.-S. and Chiu, Y.-H. (2016). Application of multiobjective topology optimization to miniature ultrawideband antennas with enhanced pulse preservation. *IEEE Antennas and Wireless Propagation Letters*, 15:842–845.
- [Colagrande et al., 2011] Colagrande, S., Ranalli, D., and Tallini, M. (2011). Ground Penetrating Radar Assessment of Flexible Road Pavement Degradation. *International Journal of Geophysics*, 2011:1–11.
- [Deb et al., 2002] Deb, K., Pratap, A., Agarwal, S., and Meyarivan, T. (2002). A fast and elitist multiobjective genetic algorithm: Nsga-ii. *IEEE transactions on evolutionary computation*, 6(2):182–197.
- [Dérobert et al., 2008] Dérobert, X., Iaquinta, J., Klysz, G., and Balayssac, J.-P. (2008). Use of capacitive and GPR techniques for the non-destructive evaluation of cover concrete. *NDT & E International*, 41(1):44–52.
- [Dumoulin et al., 2012] Dumoulin, A., John, M., Ammann, M. J., and McEvoy, P. (2012). Optimized monopole and dipole antennas for uwb asset tag location systems. *IEEE Transactions on Antennas and Propagation*, 60(6):2896–2904.
- [Elmansouri et al., 2012] Elmansouri, M. A., Radway, M. J., and Filipovic, D. S. (2012). Frequency-and time-domain performance of four-arm mode-2 spiral antennas. *IEEE transactions on antennas and propagation*, 60(6):2627–2634.
- [Elsheakh and Abdallah, 2019] Elsheakh, D. N. and Abdallah, E. A. (2019). Compact ultra-wideband vivaldi antenna for ground-penetrating radar detection applications. *Microwave and Optical Technology Letters*, 61(5):1268–1277.
- [Elsherbeni and Demir, 2016] Elsherbeni, A. Z. and Demir, V. (2016). *The finite-difference time-domain method for electromagnetics with MATLAB simulations*. The Institution of Engineering and Technology.
- [Faraji et al., 2009] Faraji, H., Moini, R., Sadeghi, S., and Talebi, H. (2009). Design of a new wire bow-tie antenna for ultrawide-band GPR applications using multiobjective genetic algorithm. In *2009 13th International Symposium on Antenna Technology and Applied Electromagnetics and the Canadian Radio Science Meeting*, pages 1–4. IEEE.

- [Fernandes et al., 2017] Fernandes, F. M., Fernandes, A., and Pais, J. (2017). Assessment of the density and moisture content of asphalt mixtures of road pavements. *Construction and Building Materials*, 154:1216–1225.
- [Gibson, 1979] Gibson, P. (1979). The vivaldi aerial. In *1979 9th European Microwave Conference*, pages 101–105. IEEE.
- [Guo et al., 2019] Guo, J., Tong, J., Zhao, Q., Jiao, J., Huo, J., and Ma, C. (2019). An ultrawide band antipodal vivaldi antenna for airborne GPR application. *IEEE Geoscience and Remote Sensing Letters*, 16(10):1560–1564.
- [Hassan et al., 2014] Hassan, E., Wadbro, E., and Berggren, M. (2014). Topology optimization of metallic antennas. *IEEE transactions on antennas and propagation*, 62(5):2488–2500.
- [Hidalgo et al., 2010] Hidalgo, C., Pandales, C. A., Pedroza, B. A., and Rodriguez, M. A. (2010). Comportamiento de una pista experimental de pavimento flexible con base estabilizada con cal. *Revista Ingenierias Universidad de Medellin*, 9(16):37–47.
- [Huisman et al., 2001] Huisman, J., Sperl, C., Bouten, W., and Verstraten, J. (2001). Soil water content measurements at different scales: accuracy of time domain reflectometry and ground-penetrating radar. *Journal of Hydrology*, 245(1-4):48–58.
- [IEEE, 2017] IEEE (2017). IEEE standard for radar definitions. *IEEE Std 686TM-2017*.
- [Islam et al., 2008] Islam, M. T., Shakib, M. N., Misran, N., and Yatim, B. (2008). Analysis of broadband slotted microstrip patch antenna. In *Proceedings of 11th International Conference on Computer and Information Technology, ICCIT*, pages 758–761.
- [Jol, 2010] Jol, H. M. (2010). *Ground Penetrating Radar: Theory and Applications*. Elsevier.
- [Kanda, 1983] Kanda, M. (1983). Time domain sensors for radiated impulsive measurements. *IEEE Transactions on Antennas and Propagation*, 31(3):438–444.
- [Karim et al., 2013] Karim, M. N. A., Malek, M. F. A., Jamlos, M. F., Seng, L. Y., and Saudin, N. (2013). Design of Ground Penetrating Radar antenna for buried object detection. In *IEEE International RF and Microwave Conference, Proceedings (RFM)*, pages 253–257, Penang, Malaysia.

- [Karoui et al., 2019] Karoui, M. S., Ghariani, N., Lahiani, M., and Ghariani, H. (2019). A compact uwb elliptic antenna for indoor localization system. *IEICE Electronics Express*, pages 16–20190425.
- [Kasi and Chakrabarty, 2012] Kasi, B. and Chakrabarty, C. K. (2012). Ultra-wideband antenna array design for target detection. *Progress in Electromagnetics Research*, 25:67–79.
- [Khan et al., 2018] Khan, Z., Razzaq, A., Iqbal, J., Qamar, A., and Zubair, M. (2018). Double circular ring compact antenna for ultra-wideband applications. *IET Microwaves, Antennas & Propagation*, 12(13):2094–2097.
- [Kim and Scott, Jr., 2004] Kim, K. and Scott, Jr., W. R. (2004). A resistive linear antenna for ground-penetrating radars. In *Detection and Remediation Technologies for Mines and Minelike Targets IX*, volume 5415, pages 359–370.
- [Koziel and Bekasiewicz, 2017] Koziel, S. and Bekasiewicz, A. (2017). Comprehensive comparison of compact uwb antenna performance by means of multiobjective optimization. *IEEE Transactions on Antennas and Propagation*, 65(7):3427–3436.
- [Kumar and Maiti, 2014] Kumar, V. and Maiti, S. (2014). A novel characterization of shape of pulse in GPR signal transmission. In *2014 International Conference on Communication and Signal Processing*, pages 944–947. IEEE.
- [Kundu et al., 2018] Kundu, S., Chatterjee, A., Jana, S. K., and Parui, S. K. (2018). Gain enhancement of a printed leaf shaped uwb antenna using dual fss layers and experimental study for ground coupling GPR applications. *Microwave and Optical Technology Letters*, 60(6):1417–1423.
- [Kundu and Jana, 2018] Kundu, S. and Jana, S. K. (2018). A compact umbrella shaped uwb antenna for ground-coupling GPR applications. *Microwave and Optical Technology Letters*, 60(1):146–151.
- [Kurtz et al., 1997] Kurtz, J. L., Fisher, J. W., Skau, G., Armaghani, J., and Moxley, J. G. (1997). Advances in ground-penetrating radar for road subsurface measurements. In *Radar Sensor Technology II*, volume 3066, pages 11–22. International Society for Optics and Photonics.
- [LÁČÍK et al., 2010] LÁČÍK, J., Lager, I. E., and RAIDA, Z. (2010). Multicriteria optimization of antennas in time-domain. *Radioengineering*, 19(1):105.



- [Lahouar and Al-Qadi, 2008] Lahouar, S. and Al-Qadi, I. L. (2008). Automatic detection of multiple pavement layers from GPR data. *NDT & E International*, 41(2):69–81.
- [Lee et al., 2005] Lee, S. H., Park, J. K., and Lee, J. N. (2005). A novel cpw-fed ultra-wideband antenna design. *Microwave and Optical Technology Letters*, 44(5):393–396.
- [Leng and Al-Qadi, 2014] Leng, Z. and Al-Qadi, I. L. (2014). An innovative method for measuring pavement dielectric constant using the extended cmp method with two air-coupled GPR systems. *NDT & e International*, 66:90–98.
- [Lestari et al., 2010] Lestari, A. A., Bharata, E., Suksmono, A. B., Kurniawan, A., Yarovoy, A. G., and Ligthart, L. P. (2010). A modified bow-tie antenna for improved pulse radiation. *IEEE Transactions on Antennas and Propagation*, 58(7):2184–2192.
- [Li and Luk, 2014] Li, Y. and Luk, K.-M. (2014). Low-cost high-gain and broadband substrate-integrated-waveguide-fed patch antenna array for 60-Ghz band. *IEEE Transactions on Antennas and Propagation*, 62(11):5531–5538.
- [Lin et al., 2008] Lin, W.-B., Liu, Y.-T., and Chen, F.-C. (2008). A new ultra-wideband monocycle pulse generator using second-order transient circuit. In *2008 38th European Microwave Conference*, pages 1585–1588. IEEE.
- [Liu and Sato, 2014] Liu, H. and Sato, M. (2014). In situ measurement of pavement thickness and dielectric permittivity by GPR using an antenna array. *NDT & E International*, 64:65–71.
- [Liu et al., 2014] Liu, S., Wang, Q., and Gao, R. (2014). A topology optimization method for design of small GPR antennas. *Structural and Multidisciplinary Optimization*, 50(6):1165–1174.
- [Loizos and Plati, 2007] Loizos, A. and Plati, C. (2007). Accuracy of pavement thicknesses estimation using different ground penetrating radar analysis approaches. *NDT & E International*, 40(2):147–157.
- [Loulizi et al., 2003] Loulizi, A., Al-Qadi, I. L., and Lahouar, S. (2003). Optimization of ground-penetrating radar data to predict layer thicknesses in flexible pavements. *Journal of transportation engineering*, 129(1):93–99.
- [Maharaj and Leyland, 2010] Maharaj, A. and Leyland, R. (2010). The dielectric constant as a means of assessing the properties of road construction materials. In *Pro-*

- ceedings of the 29th Southern African Transport Conference (SATC)*, volume 0001, pages 487–498, Pretoria.
- [Marler and Arora, 2010] Marler, R. T. and Arora, J. S. (2010). The weighted sum method for multi-objective optimization: new insights. *Structural and multidisciplinary optimization*, 41(6):853–862.
- [Moreno de Jong van Coevorden et al., 2013] Moreno de Jong van Coevorden, C., Pantoja, M. F., García, S. G., Bretones, A. R., Gomez-Martin, R., and Palmer, K. (2013). Multiobjective-optimized design of a new uwb antenna for uwb applications. *International Journal of Antennas and Propagation*, 2013.
- [Ng et al., 2015] Ng, K.-B., Chan, C. H., and Luk, K.-M. (2015). Low-cost vertical patch antenna with wide axial-ratio beamwidth for handheld satellite communications terminals. *IEEE Transactions on Antennas and Propagation*, 63(4):1417–1424.
- [Nobes, 2017] Nobes, D. C. (2017). Ground penetrating radar response from voids: A demonstration using a simple model. *NDT & E International*, 91:47–53.
- [Oliveira et al., 2016] Oliveira, D. B., Lisboa, A. C., Fonseca, L. A., Silva, E. J., and Adriano, R. (2016). Low-cost antenna design for RFID readers using multiobjective optimization. *Microwave and Optical Technology Letters*, 58(4):905–908.
- [Oliveira et al., 2014] Oliveira, D. B., Vieira, D. A., Lisboa, A. C., and Goulart, F. (2014). A well posed inverse problem for automatic pavement parameter estimation based on GPR data. *NDT & E International*, 65:22–27.
- [Omar et al., 2013] Omar, A., Qaroot, A., and Scardelletti, M. (2013). UWB coplanar-waveguide-fed spiral slot antenna. In *7th European Conference on Antennas and Propagation (EuCAP)*, pages 2901–2902, Gothenburg, Sweden.
- [Orrillo et al., 2010] Orrillo, H., Tavares, S., Pantaleon, C., and Kofuji, S. (2010). Effect of the substrate on the performance of corrugated UWB antennas. In *IEEE Latin-American Conference on Communications*.
- [Pérez-Gracia et al., 2008] Pérez-Gracia, V., González-Drigo, R., and Di Capua, D. (2008). Horizontal resolution in a non-destructive shallow GPR survey: An experimental evaluation. *NDT & E International*, 41(8):611–620.
- [Price et al., 2006] Price, K., Storn, R. M., and Lampinen, J. A. (2006). *Differential evolution: a practical approach to global optimization*. Springer Science & Business Media.

- [Qing et al., 2006] Qing, X., Chen, Z. N., and Chia, M. Y. W. (2006). Characterization of ultrawideband antennas using transfer functions. *Radio science*, 41(01):1–10.
- [Queiroz et al., 2013] Queiroz, F., Vieira, D., and Travassos, X. (2013). Analyzing the relevant features of GPR scattered waves in time-and frequency-domain. *Research in Nondestructive Evaluation*, 24(2):105–123.
- [Quintero et al., 2011] Quintero, G., Zurcher, J.-F., and Skrivervik, A. K. (2011). System fidelity factor: A new method for comparing uwb antennas. *IEEE Transactions on Antennas and Propagation*, 59(7):2502–2512.
- [Saarenketo and Scullion, 2000] Saarenketo, T. and Scullion, T. (2000). Road evaluation with ground penetrating radar. *Journal of Applied Geophysics*, 43(2-4):119–138.
- [Shao et al., 2013] Shao, J., Fang, G., Ji, Y., Tan, K., and Yin, H. (2013). A novel compact tapered-slot antenna for GPR applications. *IEEE antennas and wireless propagation letters*, 12:972–975.
- [Sheng et al., 2003] Sheng, H., Orlik, P., Haimovich, A. M., Cimini, L. J., and Zhang, J. (2003). On the spectral and power requirements for ultra-wideband transmission. In *IEEE International Conference on Communications, 2003. ICC'03.*, volume 1, pages 738–742. IEEE.
- [Spagnolini, 1997] Spagnolini, U. (1997). Permittivity Measurements of Multilayered Media With Monostatic Pulse Radar. *IEEE Transactions on Geoscience and Remote Sensing*, 35(2):454–463.
- [Sun et al., 2021] Sun, H.-H., Lee, Y. H., Luo, W., Ow, L. F., Yusof, M. L. M., and Yucel, A. C. (2021). Compact dual-polarized vivaldi antenna with high gain and high polarization purity for gpr applications. *Sensors*, 21(2):503.
- [Telzhensky and Leviatan, 2006] Telzhensky, N. and Leviatan, Y. (2006). Novel method of UWB antenna optimization for specified input signal forms by means of genetic algorithm. *IEEE Transactions on Antennas and Propagation*, 54(8):2216–2225.
- [Travassos et al., 2012] Travassos, X., Vieira, D., and Lisboa, A. (2012). Antenna optimization using multiobjective algorithms. *ISRN Communications and Networking*, 2012.
- [Travassos Jr et al., 2018] Travassos Jr, X., Avila, S., Adriano, R. d. S., and Ida, N. (2018). A review of ground penetrating radar antenna design and optimization.

- Journal of Microwaves, Optoelectronics and Electromagnetic Applications (JMoe)*, 17(3):385–402.
- [Uduwawala, 2007] Uduwawala, D. (2007). Gaussian vs differentiated gaussian as the input pulse for ground penetrating radar applications. In *2007 International Conference on Industrial and Information Systems*, pages 199–202. IEEE.
- [Valadão, 2020] Valadão, M. A. C. (2020). *Proposta de Um Algoritmo Evolutivo Assistido por um Modelo de Aproximação Kriging para Problemas de Otimização de Alto Custo Computacional*. PhD thesis, Universidade Federal de Minas Gerais.
- [Van Coevorden et al., 2006] Van Coevorden, C. M. J., Bretones, A. R., Pantoja, M. F., Ruiz, F. J., García, S. G., and Martin, R. G. (2006). Ga design of a thin-wire bow-tie antenna for GPR applications. *IEEE Transactions on Geoscience and Remote Sensing*, 44(4):1004–1010.
- [Van Der Kruk et al., 2007] Van Der Kruk, J., Arcone, S. A., and Liu, L. (2007). Fundamental and higher mode inversion of dispersed GPR waves propagating in an ice layer. *IEEE Transactions on geoscience and remote sensing*, 45(8):2483–2491.
- [Wang, 2015] Wang, Y. (2015). Frequencies of the Ricker wavelet. *Geophysics*, 80(2):31–37.
- [Xie et al., 2011] Xie, Z.-m., Li, Y., and Ding, H.-h. (2011). Time-domain optimization for uwb antenna based on correlated energy gain. *Microwave and Optical Technology Letters*, 53(1):97–102.
- [Yang et al., 2008] Yang, Y., Wang, Y., and Fathy, A. E. (2008). Design of compact vivaldi antenna arrays for uwb see through wall applications. *Progress In Electromagnetics Research*, 82:401–418.
- [Yang, JianKishk, 2011] Yang, JianKishk, A. (2011). The Self-Grounded Bow-Tie Antenna. In *IEEE International Symposium on Antennas and Propagation*, pages 1452–1455, Spokane, USA.
- [Zhao et al., 2014] Zhao, J.-y., Zhang, Z.-y., Liu, N.-w., Fu, G., and Gong, S.-x. (2014). Wideband Unidirectional Bowtie Antenna with Pattern Improvement. *Progress In Electromagnetics Research Letters*, 44(January):119–124.
- [Zhao and Al-Qadi, 2016] Zhao, S. and Al-Qadi, I. L. (2016). Development of an analytic approach utilizing the extended common midpoint method to estimate asphalt

- pavement thickness with 3-d ground-penetrating radar. *NDT & E International*, 78:29–36.
- [Zhao et al., 2015] Zhao, S., Shangguan, P., and Al-Qadi, I. L. (2015). Application of regularized deconvolution technique for predicting pavement thin layer thicknesses from ground penetrating radar data. *Ndt & E International*, 73:1–7.
- [Zhou and Cui, 2011] Zhou, B. and Cui, T. J. (2011). Directivity Enhancement to Vivaldi Antennas Using Compactly Anisotropic Zero-Index Metamaterials. *IEEE Antennas and Wireless Propagation Letters*, 10:326–329.